



OPEN Enhancing the backstepping control approach competencies for wind turbine systems using a dual star induction generator

Abdessmad Milles¹, Elkheir Merabet¹, Habib Benbouhenni^{2✉}, Ilhami Colak³, Nouredine Bensedira⁴, Naamane Debouché⁵, Mohammed-Salah Aggoune⁴ & Ghoulmallah Boukhalifa⁴

The goal of this study is to present a novel and improved backstepping control (BC) technique for a dual-star induction generator (DSIG) powered by a wind turbine. This approach relies on the ant lion optimization (ALO), which is employed to determine the optimal parameters of the BC approach and improve the performance of the wind conversion energy system. The ALO approach enhances the robustness of the DSIG, enabling faster dynamic responses, greater accuracy, and consistently improved effectiveness. The fitness function of the ALO approach integrates both integral time absolute error and integral time squared error criteria, ensuring the fulfillment of effectiveness objectives. The performance of the BC-ALO approach is validated through MATLAB. The results of the tests show that the new approach reduces total harmonic distortion, minimizes stator energy fluctuations, and improves dynamic efficiency compared to the BC approach. Additionally, the method can handle uncertainties in model parameters, making it versatile and practical. Simulation results show that the BC-ALO method reduces the total harmonic distortion value compared to the BC method by percentages estimated at 29.45%, 50.44%, and 43.10% in all tests. Also, this approach improves the overshoot value of DSIG power compared to the traditional BC strategy by an estimated 100% in all tests. The proposed approach improves the response time value of the reactive power compared to the conventional BC strategy by percentages estimated at 97.65%, 97.78%, and 95.23% in all tests. The DC link voltage ripples are low if the proposed approach is used, with ratios estimated at 63.31%, 71.38%, and 71.89% in all tests. These results make the proposed approach interesting in other applications such as photovoltaic systems.

Keywords Dual-star induction generator, Integral time squared error, Backstepping control, Ant lion optimization, Integral time absolute error

List of symbols

BC	Backstepping control
DSIG	Dual-star induction generators
IM	Induction machine
SM	Synchronous machine
THD	Total harmonic distortion
WS	Wind speed
MPM	Multiphase machine
STSMC	Super twisting sliding mode control
PI	Proportional–integral controller
DTC	Direct torque control
DR	Dynamic response

¹Laboratory of Materials Physics, Radiation and Nanostructures (LPMRN), Faculty of Technology, University of Bordj Bou Arreridj, 34265 Bordj Bou Arreridj, Algeria. ²Laboratoire LAAS, Department of Electrical Engineering, Ecole Nationale Polytechnique d'Oran, Bp 1523 EL M'naouer, Oran, Algeria. ³Department of Electrical and Electronics Engineering, Istinye University, Istanbul, Turkey. ⁴University of Batna 2, Batna, Algeria. ⁵Brothers Mentouri University, Constantine, Algeria. ✉email: habib.benbouhenni@enp-oran.dz

SPOF	Single-phase open fault
T_{em}	Electromagnetic torque
P_s	Active power
MC	Matrix converter
TOSTC	Third-order super-twisting controller
SMC	Sliding mode control
AI	Artificial intelligence
GWO	Grey wolf optimization
V_s	Stator voltage
M_s	Mutual inductance
J	Inertia
I_{qs} and I_{ds}	Stator currents in the d - q reference frame
V_{qs} and V_{ds}	Voltages of the stator in the d - q reference frame
ω_{qs}	Electrical pulsation of the stator
f_s	Viscous friction
p	Number of pole pairs
φ_{qs} and φ_{ds}	Flux of the stator in the d - q reference frame
R	Radius blade
σ	Dispersion coefficient
L_r and L_s	Rotor and stator inductance
WE	Wind energy
RPS	Renewable power source
ALO	Ant lion optimization
MPPT	Maximum power point tracking
EW	Energy winding
CW	Control winding
FOC	Field-oriented control
IG	Induction generator
DSIM	Double-star induction machine
MM	Mathematical model
PWM	Pulse width modulation
Q_s	Reactive power
C_p	Coefficient of power
λ	Tep speed ratio
OPF	Open phase fault
VC	Vector control
NN	Neural network
VRV	Voltage reference value
DSIM	Double star induction machine
f_s	Stator frequency
g	Slip
ω_r	Electrical pulsation of the rotor
φ_{qr} and φ_{dr}	Flux of the rotor in the d - q reference frame
V_{qr} and V_{dr}	Voltages of the rotor in the d - q reference frame
Ω	Mechanical rotor speed
P_s^*	Reference of active power
ρ	Air density
I_{qr} and I_{dr}	Rotor currents in the d - q reference frame
Ω_t	Mechanical speed of turbine
β	Pitch angle
R_r, R_s	Rotor and stator resistance

Among other renewable power sources (RPSs), wind energy (WE) is a rapidly growing sector¹. It is one of the most well-known types of clean RPSs and is widely available worldwide, especially in rural areas. Its cost-effectiveness and availability make it a popular choice². However, this approach has several drawbacks, such as intermittency and the need for a large land area and significant investment. Its initial use was for mechanical applications, such as water pumping, before being harnessed for electricity production³. Nevertheless, induction machines (IMs) are widely applied across various fields and serve numerous purposes, particularly in WE conversion systems. They are important sources for the production of electrical energy. Additionally, controlling them is complex and often difficult because their feed is through fixed components with both excitation and generation functions. This limits their use and makes them only suitable for producing electricity from wind turbines (WTs) or hydroelectric generators in isolated systems^{1,3}.

Regarding the topic of WE production, several machines can be used for generating power, such as synchronous machines (SMs)⁴, direct current (DC) machines⁵, IMs⁶, and multiphase machines⁷. The latter can be used to generate energy, as they are used in cases with high energy and have advantages that differ from those of traditional machines. Dual-star induction generators (DSIGs) are multiphase machines (MPMs) in which two symmetrical parts are used at an angular difference of 30° or 60°⁸. MPMs, such as those with seven or five phases, can also be used since more poles equate to more torque and, thus, more power production, which is a positive outcome. In Ref.⁹, electrical energy was produced from a WE using a DSIG-type machine, which was

controlled by a control based on a proportional-integral (PI) regulator. Furthermore, the reference value for active power (P_s) was obtained by using the maximum power point (MPP) tracking (MPPT) approach, which links P_s to changes in the wind speed (WS) curve. In Ref.¹⁰, an experimental research study was conducted on a DSIG placed in a wind energy conversion system (WECS), and the empirical results verified the suitability of the DSIG for generating electrical energy. DSIGs possess advantages that make them better suited for increased use compared to induction generators (IGs), such as reduced rotor current total harmonic distortion (THD), good energy efficiency, power splitting, low maintenance costs, and the ability to use them at a constant or variable speed, as required¹¹. In Ref.¹², the author presented a generalized model to study the characteristics of a DSIG based on a three-phase variable, where the mathematical model (MM) of the DSIG was given using mechanical and electrical equations. The author considered that DSIG is a three-phase network, as using DSIG leads to obtaining two three-phase networks. In Ref.¹³, another form of DSIG was given for generating power from WE, where the analysis and design of a brushless DSIG for generating current was presented. The advantage of this new generator is that it differs from DSIG in terms of the use of brushless materials to improve robustness and reduce regular maintenance. The results show the excellent effectiveness of this suggested generator with variable WS. Another type of dual-star machine was proposed in Ref.¹⁴, specifically, dual-star permanent-magnet SMs were used to generate EE from the WE. This type of MPM relies on the use of SMs and is therefore different from DSIG in terms of the working principle and costs of generating electricity. Furthermore, the author provided a method for determining the value of the inductance parameters for this new machine and performed a simulation in MATLAB. The simulation was conducted under varying WS, demonstrating the high efficiency of this generator in producing energy even under fluctuating conditions. In Ref.¹⁵, dual star induction machines (DSIMs) are of great importance as they are one of the most reliable solutions in the industrial field, especially in electrical transmission and power generation systems. The use of DSIMs allows for fault-tolerant operation, which makes them suitable for the field of electrical power generation. In Ref.¹⁶, the application of DSIM for powertrain for electric vehicles is discussed. DSIM has been used as a promising option due to its significant advantages in terms of performance, power efficiency, and reliability. This system could play a major role in the development of electric vehicle technology and other applications. The author argues that the use of DSIM machines reduces electromagnetic torque fluctuations, limits current harmonics, and improves power factor compared to three-phase machines. Sliding mode control was used to control this machine, and the proposed system was implemented in MATLAB. The results showed that DSIM improves the overall performance and efficiency of electric vehicles, especially in traction and braking modes, underscoring the importance of DSIM in the sustainable development of electric transportation systems.

In Ref.¹⁷, the author conducted an evaluation study of the performance and effectiveness of multiphase IGs within a grid-connected standalone WT system, and the study specifically focused on DSIGs. MATLAB was used to complete this study using variable WS. Therefore, based on this completed research study, these generators have achieved excellent performance under different working conditions to generate energy from WE, and the power quality is considered fairly acceptable. The use of MPMs increases a system's complexity compared to three-phase machines considering the cost, maintenance, and degree of control; notably, simple and easy-to-implement controls are used to reduce costs and burdens. In Ref.¹⁸, the author argues that DSIG is in increasing use in the field of renewable energies due to its advantages in improving reliability and dividing supply. This generator was used in a wind energy conversion system with variable-speed wind turbines. In this work, the author studied the effect of changing the electrical angle between the two stator windings of a generator in reducing the value of harmonic distortion and power quality. This study was carried out in MATLAB, and these results showed the extent of the effect of this angle on the quality of current and power.

DSIGs can be regulated through various strategies, such as vector controls (VCs) and field-oriented controls (FOCs). Operations aimed at controlling the P_s and reactive power (Q_s) of DSIGs can be performed^{3,8}. Nonetheless, a precise definition of DSIG parameters is imperative in the proposed controller concept¹⁹. In Ref.²⁰, a DSIG control was proposed based on the use of an air-gap flux-oriented control to generate power from a WT system, where a 13-region time-optimized space vector-based hybrid bus clamping approach with pulse width modulation (PWM) was used. The proposed control is based on the FOC strategy, making the approach dependent on the DSIG parameters. Its significant drawbacks are its high complexity and high cost. However, its high robustness and excellent performance are its key features. MATLAB and experimental work were used to validate the effectiveness of this approach. The experimental results demonstrated high accuracy and significant efficiency in improving power quality compared to the traditional approach.

Classical VC systems based on control instruments are used to control IMs in many applications in power production. This is because they have uncomplicated and simple designs, are easy to implement, and can separate P_s and Q_s well^{8,19}. However, their use is limited due to the dependence of the effectiveness of the VC process on the tuning of the PI²¹. In Ref.²², the authors used a stator flux-oriented VC technique to control the power output from the DSIG, and an 11-zone hybrid PWM technique was used to create the desired control pulses. The benefits of using this proposed method are the low complexity and the use of system parameters, which make the method sensitive to changes in DSIG parameters. MATLAB was used to verify this control scheme, and the results showed the presence of fluctuations at various current and power levels. Thus, another technique that can be used to control DSIG and is highly effective and efficient for improving the quality of the resulting energy was explored. In Ref.²³, the use of super-twisting continuous sliding mode controllers (STCSMC) has been proposed as a suitable solution to overcome the drawbacks of the VC technique of DSIG. In this proposed approach, an STCSMC controller is used to control the power, allowing for improved power and current quality compared to conventional controllers. In addition to the STCSMC controller, a PWM strategy is used to control the machine's inverter. This proposed strategy is implemented in MATLAB, using variable winding to study the behavior. The results show that the STCSMC controller significantly improves performance and robustness compared to the conventional approach, as demonstrated by reduced power ripples and current THD.

Another approach is direct torque control (DTC), which is used to control DSIMs by utilizing a matrix converter (MC) in a variable-WS turbine system²⁴. MC was used to compensate for the deficiencies of the traditional back-to-back inverter and improve the characteristics of the DTC technique to reduce torque fluctuations and enhance the current quality. Results using MATLAB showed the competence of the designed control in terms of enhancing system efficacy under different working conditions. Because this process uses system characteristics, which alter control in the event of an unfavorable system breakdown, using the DTC approach to manage the DSIG necessitates the employment of estimation procedures for both torque and flux. In Ref.²⁵, a novel control concept was adopted for DSIGs, and the producer system was divided into two subsystems to be analyzed independently. The machine had 12 phases and a rectified load. The network equation set was constructed using the loop current technique in terms of network graph theory. By using a fixed time step and a changing time step alternately to solve the numerical stability problem, voltage and current were produced, and the corresponding essential power profile components were obtained. Among the other IG subsystems with dual-stator winding and solid cage rotors, the electromagnetic area analysis technique and multivariate optimization technique have been combined to obtain the control coil current and stator frequency. In Ref.²⁶, neural networks (NNs) and the FOC technique were combined to control the energy generated by DSIGs. In this paper, the MPPT was used to determine the reference value of P_s , and a PWM was used to control the run of the inverter. The NN-FOC approach differs from the DTC and FOC techniques because it replaces all PI controllers with an NN controller. MATLAB was used to realize the suggested method, and the results were compared with those of the FOC-PI approach. The results showed the efficacy of the designed approach in terms of current quality and significantly enhanced the features of the studied system. The author in Ref.²⁷ believes that the use of DSIG allows for eliminating the defects of the slip ring device. Also, using this machine has another advantage: it gives better power quality compared to using a DFIG generator. It is also possible to use a PI-type controller to control the power, which allows the control system to be simplified and costs reduced. In Ref.²⁸, the modeling and analysis of a DSIG with no identical coefficients was performed in a new way. The DSIG was controlled using the FOC strategy, where a battery was used to store the resulting power and use it when necessary. A steady-state model was developed, and the control performance was demonstrated under different working conditions, where the control was studied in the case of variable WS. The results demonstrated the elevated effectiveness of the suggested system in generating and storing power. In Ref.²⁹, a power control strategy is proposed to improve the DSIG characteristics. An asynchronous reference frame is used to model the DSIG. This proposed strategy was implemented using simulation and experimental work, where a DC motor was used to drive the DSIG at different speeds. The obtained results demonstrate the efficiency and accuracy of the DC bus voltage across various operating conditions. In Ref.³⁰, a new strategy for controlling networked DSIGs was proposed. The proposed control relied on the use of both the backstepping control (BC) and FOC to regulate the energy created by the system and reduce current fluctuations. DSIGs have many advantages, such as high reliability and a split supply, which make them suitable for generation systems; therefore, it is needed to use a control system with high effectiveness. This research study aims to overcome the problems resulting from the use of PI controllers. Notably, a new and different FOC approach in which the BC technique is applied to replace the PI controller and regulate the Q_s and P_s of DSIGs is explored. This approach has the advantages of being long-lasting and performing exceptionally well in terms of reducing fluctuations and enhancing current quality. However, this control's drawback is its complexity and the abundance of control parameters, which make it computationally difficult to adjust. Furthermore, since this control approach is dependent on the system characteristics, it is undesirable to alter the DSIG parameters since they will impact the system. A comparison between SMC strategy and third-order super-twisting controller (TOSTC) strategy for controlling DSIGs was proposed³¹. Both approaches were tested under phase faults. Simulation results demonstrated the effectiveness of the TOSTC approach compared to SMC in reducing the chatter phenomenon and significantly improving power quality. Furthermore, the TOSTC approach significantly reduces the THD value under phase faults. Despite its high performance, the TOSTC approach has drawbacks: power and current ripples persist. These ripples are observed to be significantly higher in robustness testing. In Ref.³², an IT2FL controller, coupled with PWM technique, was used to control the DSIG power. High robustness and excellent performance are the key features of the proposed approach. The proposed approach was implemented in MATLAB, and the results demonstrated its effectiveness compared to other methods in improving system properties. This strategy has drawbacks, including its reliance on estimating capabilities and the presence of a significant number of gains. Furthermore, the number of rules is one of the most significant drawbacks of using the IT2FL approach, as it relies primarily on experience and experimentation. A new VC strategy was used in Ref.³³ to regulate the energies of the DSIG, where a space vector-based advanced 9-zone hybrid PWM technique was used for this purpose. This designed approach is described by its high performance and its great ability to significantly ameliorate the quality of the current. This control was realized in MATLAB using numerous tests, with results compared to the BC technique. The results showed that this designed control has a distinctive and effective performance, and this is shown by the THD of current and energy ripples. Complexity, high cost, and difficulty of implementation are the main drawbacks that limit the spread of this approach.

Traditionally, the BC approach is one of the most well-liked nonlinear control methods and has been suggested to overcome the drawbacks of the SMC technique. This control greatly increases the robustness of systems and increases the performance of various strategies. This approach has been used to control IMs³⁴, SMs³⁵, and doubly-fed induction generators³⁶. In Ref.³⁷, the BC approach and third-order SMC were combined to control an IM, and a comparison with the FOC technique was studied. The results showed the elevated efficacy of the designed approach in improving machine features compared to the FOC approach. Rooted tree optimization was used to improve the effectiveness of the BC approach of DFIGs³⁸. The findings, compared to those of the FOC technique, demonstrate that the application of this algorithm increased the efficiency and robustness of the BC approach. In Ref.³⁹, The BC strategy has been proposed as a suitable solution for controlling multi-rotor turbine systems. In

this approach, the PWM strategy is used to generate drive pulses in the inverter. The approach was implemented using MATLAB, and its performance was compared with the DPC approach. Simulation results revealed that the BC approach outperformed the DPC approach in terms of reducing fluctuations and total harmonic distortion of the current. However, the DPC approach provided a better response time (RT) than the BC approach.

Another study addressed the use of the BC approach to control a photovoltaic system⁴⁰. This study investigated the effectiveness of using the integral BC approach in improving power quality and current. The results of the integral BC approach were compared with those of a PI controller-based approach. The results demonstrated that the proposed approach outperformed other techniques in terms of improving current THD reduction and reducing Ps fluctuations. In Ref.⁴¹, a nonsingular terminal sliding mode surface strategy-based BC technique is proposed for the power control of DFIGs. This strategy has several advantages, such as high robustness and superior performance compared to conventional approaches. The performance of the proposed approach is verified using MATLAB and compared with the BC approach. The results show that the proposed approach significantly improves the power quality. However, this approach has drawbacks, including its high complexity and significant number of gains. Another solution was used in Ref.⁴² to augment the effectiveness of the BC approach in a DFIG, where an integral action scheme was used as a suitable solution. This designed control was used to control energy and determine VRVs. The PWM technique was used to transfer these values into pulses to run the machine's inverter. Therefore, this approach is described by high robustness, competence in minimizing power fluctuations, and outstanding performance compared to conventional strategies. This approach was realized in MATLAB and compared with the DPC approach and other existing methods in terms of ripples, current THD, and overshoot. The results obtained show the efficiency of this strategy and the extent of its effectiveness in improving the energy/current quality. In Ref.⁴³, the authors proposed the use of a synergetic-SMC approach to overcome the cons of the BC approach in an IM-based MRAS technique. This approach was applied to a 2-level inverter, as this approach is described by high robustness and complexity, significant gains, outstanding performance, and difficulty achieving complete implementation. Simulations were used to implement this control and compare it with FOC technique schemes in terms of the RT, fluctuation reduction ratio, and current THD. The completed comparison showed the advantage of the designed control over some existing techniques, making it a suitable solution. However, this strategy has certain disadvantages, such as a significant number of gains and high complexity, which makes it difficult to adjust the RT. Additionally, due to its reliance on the MM of the DSIG; it is affected in the event of a fault in the system, as indicated by robustness tests.

The use of artificial intelligence (AI) techniques such as genetic algorithms⁴⁴ and particle swarm optimization⁴⁵ to determine the parameters of control strategies contributes greatly to improving the characteristics of strategies and systems by minimizing power fluctuations and improving the current THD. Also, significantly increasing the robustness of the power generation system is desirable. AI techniques were used to improve the effectiveness of the BC approach, and in Ref.⁴⁶, optimization control was used to ameliorate the features of the nonlinear BC approach. The use of optimization control led to a significant augment in the efficacy of the BC approach. Many methods have been used to ameliorate the efficiency and robustness of the BC approach, such as FL techniques⁴⁷, and the FL approach was used to compensate for the gains of the BC technique. The use of the FL approach significantly increased control robustness and competence compared to those in the classical control. The cons effect of using the FL approach lies in the rules, as there is no mathematical rule to determine the best rules or best number of rules that can be used. Moreover, using FL makes the system more computationally intensive, making it an undesirable solution. In Ref.⁴⁸, both amended recurrent Romanovski polynomial NN and amended particle swarm optimization were used to overcome the cons of the BC approach. These two strategies are different in principle, as mended particle swarm optimization is used to establish the values of the gains of the BC approach and the NN approach is used to compensate for the gains; therefore, the two strategies are different in principle and application. The results showed the efficiency of the two strategies in improving the performance and efficiency of the BC approach. An NN algorithm and integral SMC approach were combined to defeat the cons of the BC technique⁴⁹. The results showed that the BC approach performed significantly better after using the NN-integral SMC technique. A NN-FL technique was used to defeat the cons of BC^{50,51}. In these research studies, the advantages of both the NN approach and the FL technique were combined to ameliorate the features of the BC approach. In Ref.⁵², the author used an adaptive NN algorithm to ameliorate the robustness of the BC technique, as the characteristics of the control were greatly improved, reflecting the efficacy of AI methods in ameliorating the control features, supporting the use of other strategies with high effectiveness, and ameliorating the features of the BC approach. Another AI approach used in Ref.⁵³ was the adaptive FL technique, which was implemented to defeat the disadvantages of the BC technique. This approach was used as a suitable solution to defeat defects and ameliorate the performance of the studied system. However, the disadvantage of this approach lies in the number of rules, which increases the system weights, which is undesirable. In a research study⁵⁴, grey wolf optimization (GWO) was used to estimate the parameters of the third-order SMC approach used to control DSIG powers. The latter is controlled by the indirect FOC approach, where MATLAB was used to realize and verify the designed control. This approach is described by complexity, difficulty of realization, a significant number of gains, and expensive. This approach was compared with the indirect FOC-SMC approach using numerous different tests, where the results showed that the approach based on the GWO algorithm has distinctive competence and high robustness compared to the indirect FOC-SMC approach. Also, the approach has a fast RT compared to the indirect FOC-SMC approach.

In this paper, DSIG is controlled using a new approach based on the use of ant lion optimizer (ALO) and BC approach. This proposed BC-ALO approach differs from the above-mentioned research studies in terms of efficacy, robustness, results, ease of realization, and cost. This proposed BC-ALO technique is used to control energy to get better competence and augment the robustness of the DSIG-based energy generation system. Therefore, the proposed BC-ALO approach is the main contribution of this paper.

The ALO algorithm is considered one of the most recent algorithms that have appeared recently, as it is not used much, especially in the field of control, which makes this research study of great importance. In this research study, the ALO algorithm was used to determine the values of the gains of the BC approach of DSIG, which makes this, research study a development and modification of the BC strategy. Therefore, this completed research study highlights the ability of the algorithm to get better the features of the BC approach of DSIG and augment the quality of power and current. MATLAB was used to realize this BC-ALO technique, comparing the efficacy and robustness of the BC approach and some research studies. Among the objectives achieved by this research study are listed the following points:

- Overcoming the problems and flaws of the approach.
- Increasing the robustness of the control system.
- Improve current and power quality.
- Underestimating the current THD.
- Improving RT to powers.
- Underestimating overshoot of DSIG power.

This paper consists of seven main sections, where the second section focuses on the mathematical modeling of the designed system for DSIGs. In the third section, the FOC technique for DSIGs is discussed, focusing on its advantages and disadvantages. The BC technique for DSIGs is described in “The BC technique” section. “Proposed BC-ALO technique” section explains the application of the BC-ALO designed in this study to control a system consisting of WTs and a DSIG. “Results” section contains the simulation results and a comparison with other research; “Conclusions” section presents the simulation results.

Modeling of the studied system

In this section, the energy system proposed for this study to generate electrical energy from wind is discussed. This studied energy system is characterized by many features that make it of great importance in the energy field, as it provides an effective solution to overcome the problem of high energy demand and the phenomenon of global warming. The use of this proposed energy system allows reducing the spread of toxic gases and thus protects the environment from pollution. The components of the studied system include a three-bladed rotor with a mechanical gearbox, a DSIG, and a grid; an LC filter; and bidirectional converters that contain a rectifier and an inverter. The control scheme includes P_s and Q_s controls, as shown in Fig. 1. The reliance of the studied energy system on a DSIG generator makes it a different system from traditional systems and a suitable solution to overcome the problem of power quality and current. As is known, DSIG has two stars. The first star acts as the energy winding (EW), which is directly attached to the electrical grid, and the second star control winding (CW) is associated with the bidirectional converters⁵⁵. The P_s and Q_s of the EW are determined for the proposed BC technique, which provides us with reliable control of the studied generator.

To study the proposed energy system, we must first address the mathematical modeling of the most prominent elements of this system. This mathematical modeling is necessary to embody the system in MATLAB. In the next subsection, the MM of the turbine is discussed with the control used to obtain the reference value for the P_s .

WT model and MPPT

To obtain electrical energy, several energy systems can be used, as these systems differ from each other in terms of the power source used. Recently, renewable sources have emerged as a promising solution to defeat the problem of rising demand for electrical energy and the problem of global warming⁵⁶. Therefore, the use of WE as a source is considered one of the most promising solutions at present and in the future. To benefit from WE, turbines are used for this purpose, as these WTs are in constant development⁵⁷. These WTs contribute significantly to protecting the environment and minimizing the costs of producing and consuming electrical energy. WTs harness the kinetic power present in WE to generate mechanical energy through the production

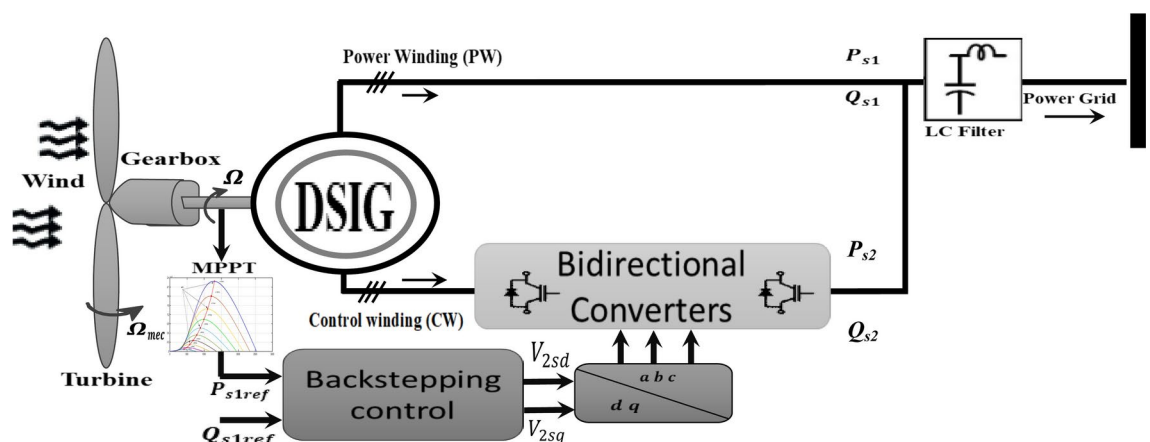


Fig. 1. The overall schematic structure of the DSIG-based wind turbine system controlled by BC technique.

of torque⁵⁸. This relationship between the WS and the mechanical energy output of WTs can be mathematically described by the following equation⁵⁹:

$$P_v = \frac{1}{2} \cdot \rho \cdot S \cdot V^3, \quad (1)$$

where ρ is the air density, P_v is the generate mechanical energy, and V is the wind speed.

The energy generated by the WT is related to the WS and a large extent to the size of the WT, as large WTs are used to get greater energy⁶⁰. As is known, these WTs are used in the form of wind farms. The MPPT-PI is often used to control the WT, as using this approach allows the resulting energy to be related to the change in WS⁶¹.

The tip speed ratio (λ) can be defined as the ratio of the linear speed of the WT blade to the WS⁶².

$$\lambda = \frac{\Omega_r \cdot R}{V}, \quad (2)$$

where R is the radius blade and Ω_r is the mechanical speed of turbine.

For the WS turbine variants, the following expression can be used to explain the energy factor expression.

$$C_p(\lambda, \beta) = 0.5109 \left(\frac{116}{\lambda_i} - 0.4\beta - 5 \right) e^{\frac{21}{\lambda_i}} + 0.0068\lambda_i, \quad (3)$$

where C_p is the coefficient of power and β is the pitch angle.

The mechanical energy recovered by a WT is written as⁶³:

$$P_{aer} = \frac{C_p}{2} \cdot \rho \cdot S \cdot V^3. \quad (4)$$

Knowing the WT speed, the aerodynamic torque can be directly determined by:

$$T_{aer} = \frac{P_{aer}}{\Omega_{turbine}} = C_p(\lambda, \beta) \times \rho \cdot S \cdot V^3 \times \frac{1}{2\Omega_{turbine}}, \quad (5)$$

where P_{aer} is the aerodynamic power and T_{aer} is the aerodynamic torque.

The total inertia is composed of the WT and DSIG inertia:

$$J = \frac{J_{turbine}}{G^2} + J_g, \quad (6)$$

where J is the total inertia, G is the gearbox, and J_g is the DSIG inertia.

To conclude the mechanical speed evolution from the total torque, electromagnetic torque was applied to the DSIG rotor. The following basic equation was applied to the dynamic system:

$$T_g - T_{em} = J \frac{d\Omega_{mec}}{dt} + f \Omega_{mec}, \quad (7)$$

where T_{em} is the electromagnetic torque, f is the friction coefficient, T_g is the DSIG torque, and Ω_{mec} is the mechanic speed.

From Fig. 2, there is a specific angular frequency at which the energy output of a WT is optimal, corresponding to the point where C_p is maximized. To achieve the optimal energy curve (MPPT curve), all the MPPs on each energy curve are linked.

Figure 3 demonstrates the relationship between C_p and λ for various values of β . The optimal values of C_p and λ can be obtained from the same figure; we note that these values are $C_{p-max}=0.48$ and $\lambda_{opt}=8.1$, respectively, for $\beta=0^\circ$ in this study.

The gearbox is used to adjust the rotational speed of the WT (slow shaft) and match the rotational speed of the DSIG (fast shaft), as shown in Fig. 4. Assuming that the gearbox is ideal (with negligible mechanical losses), we can model it using the following two expressions⁶³.

In this proposed energy system, the energy gained from the wind is used to generate power. A DSIG generator is used to convert this energy into the current. In the next subsection, the mathematical modeling of this generator is discussed, highlighting its most important characteristics.

DSIG model

DSIG is considered one of the types of asynchronous machines that can be relied upon in the field of RPSs because of its many characteristics and features, as it is considered easy to control and highly durable. Also, they are low maintenance and inexpensive compared to their counterparts. Also, DSIG is a multi-phase machine that has greater torque and can be relied upon to increase the generated power. DSIG gives greater torque than DFIG, which makes it suitable in the field of RPSs, as it has two sections: the fixed section and the moving section. Compared to DFIG, DSIG is expensive, difficult to control, and has more weight. To give the MM of DSIG, the Park transform is used for this purpose. The mechanical equation for DSIG is the same as that for DFIG. The equations that represent the electrical part are the equations that link flow, voltage, and current, where equations

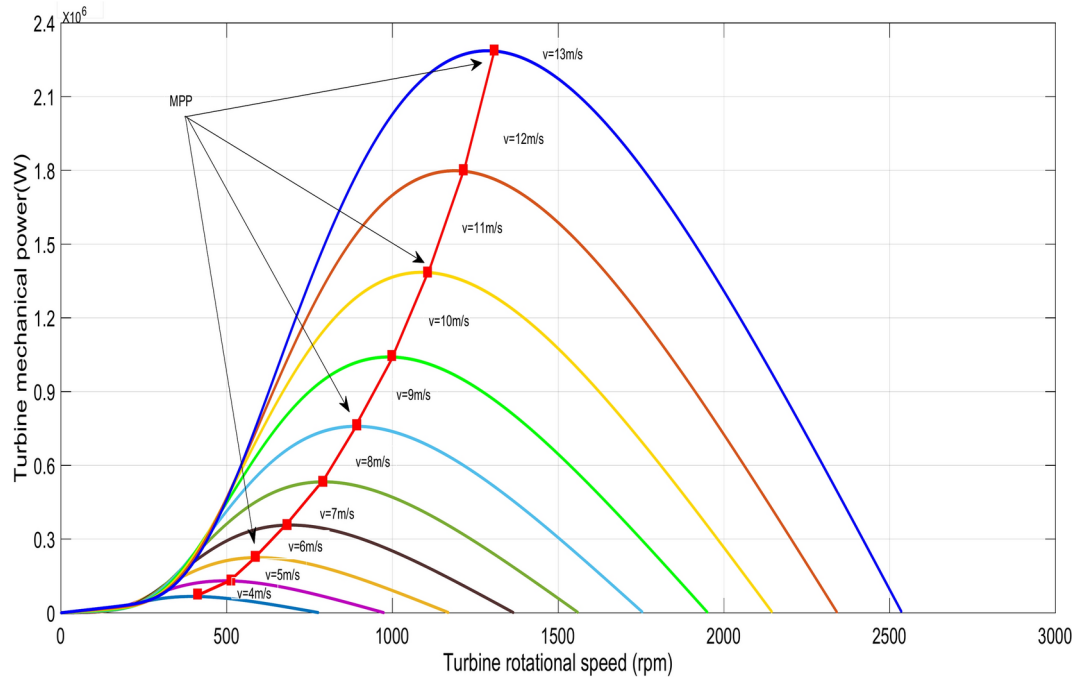


Fig. 2. Turbine power at different rotational speeds.

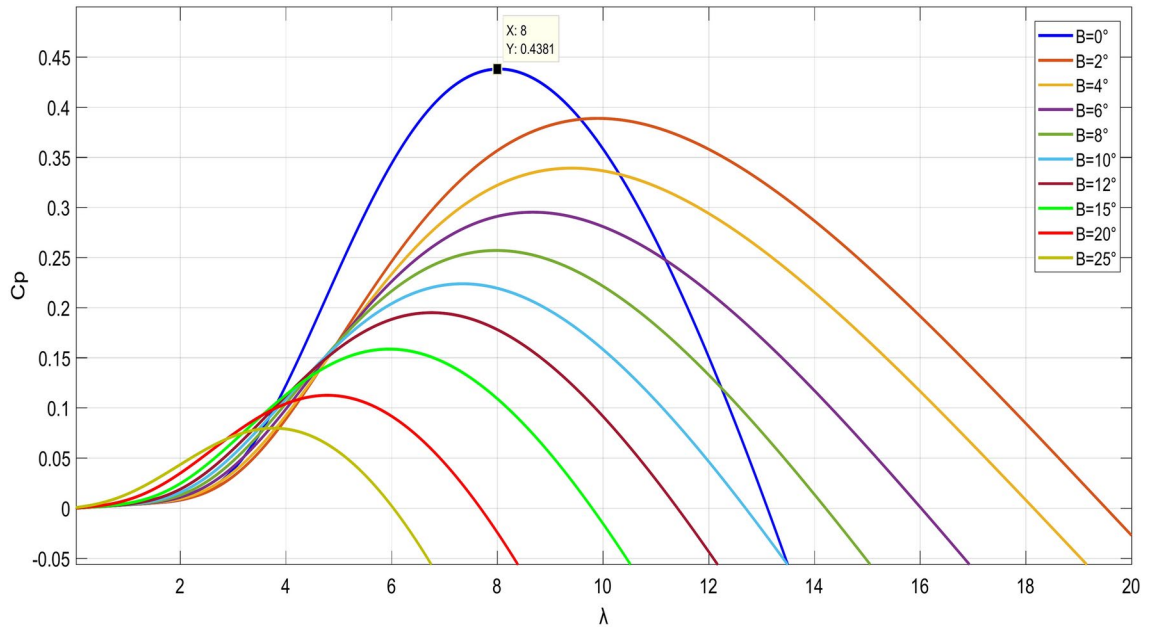


Fig. 3. Power factor as a function of rotational speed ratio.

are given for each star. The MM of the DSIG is described in the (d, q) reference frame (voltage and flux)⁶⁴ based on the following set of equations:

Stator 1

$$\begin{cases} v_{ds1} = R_{s1} \cdot i_{ds1} + \frac{d\phi_{ds1}}{dt} - \omega_{s1} \cdot \phi_{qs1} \\ v_{qs1} = R_{s1} \cdot i_{qs1} + \frac{d\phi_{qs1}}{dt} + \omega_{s1} \cdot \phi_{ds1} \end{cases}, \tag{8}$$

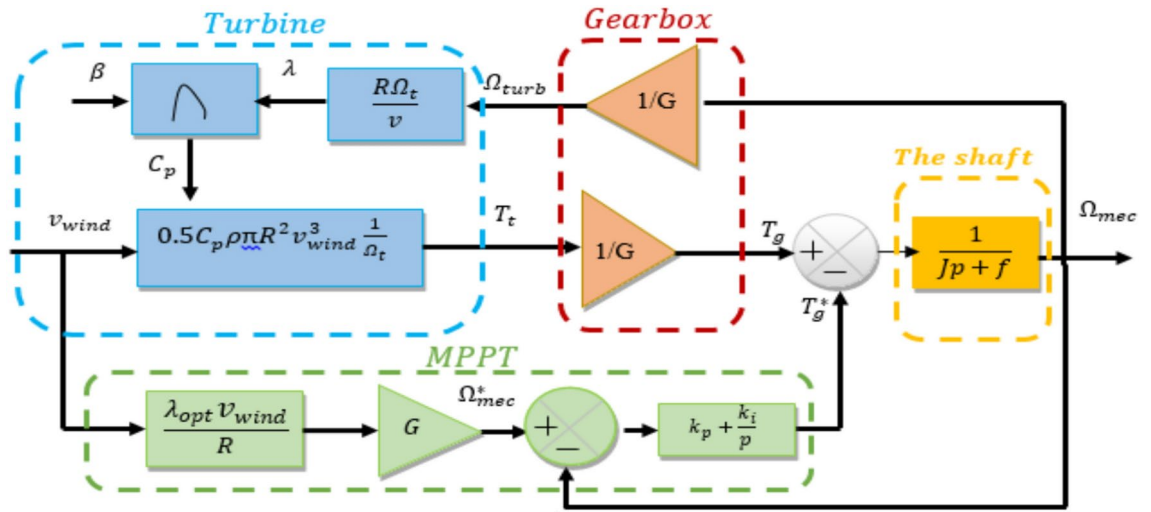


Fig. 4. Device control with speed control.

where v_{ds1} is the direct stator voltage of star 1, v_{qs1} is the quadrature stator voltage of star 1, i_{ds1} is the direct stator current of star 1, i_{qs1} is the quadrature stator current of star 1, ϕ_{ds1} is the direct stator flux of star 1, ϕ_{qs1} is the quadrature stator flux of star 1, and R_{s1} is the stator resistance of star 1.

$$\begin{cases} \phi_{ds1} = L_m(i_{ds2} + i_{dr}) + (L_{s1} + L_m)i_{ds1} \\ \phi_{qs1} = L_m(i_{qs2} + i_{qr}) + (L_{s1} + L_m)i_{qs1} \end{cases} \quad (9)$$

Stator 2

$$\begin{cases} v_{ds2} = R_{s2} \cdot i_{ds2} + \frac{d\phi_{ds2}}{dt} - \omega_{s2} \cdot \phi_{qs2} \\ v_{qs2} = R_{s2} \cdot i_{qs2} + \frac{d\phi_{qs2}}{dt} + \omega_{s2} \cdot \phi_{ds2} \end{cases}, \quad (10)$$

$$\begin{cases} \phi_{ds2} = L_m(i_{ds1} + i_{dr}) + (L_{s2} + L_m)i_{ds2} \\ \phi_{qs2} = L_m(i_{qs1} + i_{qr}) + (L_{s2} + L_m)i_{qs2} \end{cases}, \quad (11)$$

where v_{ds2} is the direct stator voltage of star 2, i_{ds2} is the direct stator current of star 2, v_{qs2} is the quadrature stator voltage of star 2, i_{qs2} is the quadrature stator current of star 2, R_{s1} is the stator resistance of star 2, ϕ_{qs2} is the quadrature stator flux of star 2, and ϕ_{ds2} is the direct stator flux of star 2.

Rotor

$$\begin{cases} v_{dr} = \frac{d\phi_{dr}}{dt} - \omega_r \cdot \phi_{qr} + R_r \cdot i_{dr} \\ v_{qr} = \frac{d\phi_{qr}}{dt} + R_r \cdot i_{qr} + \omega_r \cdot \phi_{dr} \end{cases} \quad (12)$$

where v_{dr} is the direct rotor voltage, i_{dr} is the direct rotor current, v_{qr} is the quadrature rotor voltage, i_{qr} is the quadrature rotor current, R_r is the rotor resistance, ϕ_{qr} is the quadrature rotor flux, and ϕ_{dr} is the direct rotor flux.

$$\begin{cases} \phi_{dr} = (L_r + L_m)i_{dr} + L_m(i_{ds1} + i_{ds2}) \\ \phi_{qr} = (L_r + L_m)i_{qr} + L_m(i_{qs1} + i_{qs2}) \end{cases} \quad (13)$$

where L_r is the rotor inductance.

Equation (14) shows the torque.

$$\begin{cases} v_{ds1} = R_{s1} \cdot i_{ds1} + \frac{d\phi_{ds1}}{dt} - \omega_{s1} \cdot \phi_{qs1} \\ v_{qs1} = R_{s1} \cdot i_{qs1} + \frac{d\phi_{qs1}}{dt} + \omega_{s1} \cdot \phi_{ds1} \end{cases} \quad (14)$$

where R_{s1} is the stator resistance of star 1 and ω_s is the electrical pulsation of the star 1.

In this work, the DSIG is operated as a generator only, providing power to the grid. In such a case, star 2 and star 1 have the same number of pole pairs and inherently share the same frequency. Star 2, with a pulsation value equal to ω_{s2} , induces a pulsation field equal to $g \cdot \omega_{s2}$ in the rotor. The rotor field is driven at the rotor speed, inducing a field in star 1 with a pulsation equal to the sum of the rotor field pulsation and the rotor speed ω_r .

With:

$$\omega_{s1} = \omega_{s2} = \omega_s \tag{15}$$

where ω_{s2} is the electrical pulsation of the star 2.

P_s and Q_s of the stator can be expressed as:

$$\begin{cases} P_{s1} = v_{ds1}i_{ds1} + v_{qs1}i_{qs1} \\ Q_{s1} = v_{qs1}i_{ds1} - v_{ds1}i_{qs1} \end{cases} \tag{16}$$

where P_{s1} is the active power of star 1 and Q_{s1} is the reactive power of star 1.

In the field of control, many strategies have been relied upon in the field of controlling electrical machines. The most prominent of these strategies is the mentioned FOC technique. This strategy relies on the use of a PI controller to control the characteristic quantities. In the next section, this strategy for controlling DSIG is discussed.

FOC technique for a DSIG

Conventionally, the FOC technique is considered one of the most famous strategies used in the past and is still one of the most reliable solutions to this day, as it has a fast RT. This strategy relies on the use of a PI controller, which gives it simplicity, few gains, and ease of achievement. This approach has two kinds: indirect and direct FOC strategies. The FOC technique rules are extracted from the DSIG formulations using a Park transformation that involves the rotating flux (d-q) and the stator flux orientation. Additionally, the stator flux is synchronized with the d-axis^{64,65}.

$$\begin{cases} \phi_{ds1} = \phi_s \\ \phi_{qs1} = 0 \end{cases} \Rightarrow \begin{cases} \frac{d\phi_{ds1}}{dt} = 0 \\ \phi_{qs1} = 0 \end{cases} \tag{17}$$

The Star 1 voltage equation becomes:

$$\begin{cases} v_{ds1} = R_{s1} \cdot i_{ds1} \\ v_{qs1} = R_{s1} \cdot i_{qs1} + \omega_s \cdot \phi_{ds1} \end{cases} \tag{18}$$

Assuming a stable network with a constant voltage corresponding to V_s results in a constant flux for star 1. Also, in case of neglecting the resistance of the star 1, the equations for the constant voltage can be expressed as follows:

$$\begin{cases} v_{ds1} = 0 \\ v_{qs1} = V_s = \omega_s \cdot \phi_{ds1} \end{cases} \tag{19}$$

As a result, Eqs. (12) and (13) express the rotor currents, stars 2 and 1 voltages, and star 1 energies.

$$\begin{cases} i_{dr} = -C i_{ds2} - \frac{CV_s}{\omega_s \cdot L_{s1}} \\ i_{qr} = -C i_{qs2} \end{cases} \tag{20}$$

$$\begin{cases} i_{ds1} = \left[\frac{L_m}{(L_{s1} + L_m)} (C - 1) \right] i_{ds2} + \frac{V_s}{\omega_s \cdot (L_{s1} + L_m)} \left[\frac{L_m \cdot C}{L_{s1}} + 1 \right] \\ i_{qs1} = -C i_{qs2} \end{cases} \tag{21}$$

$$\begin{cases} v_{ds2} = R_s i_{ds2} + L_s \left[1 + \frac{L_m(1-c)}{(L_s + L_m)} \right] \frac{di_{ds2}}{dt} - \omega_s L_s \left[\frac{L_m(1-C)}{(L_s + L_m)} + 1 \right] i_{qs2} \\ v_{qs2} = R_s i_{qs2} + L_s \left[1 + \frac{L_m(1-c)}{(L_s + L_m)} \right] \frac{di_{qs2}}{dt} - \omega_s L_s \left[\frac{L_m(1-C)}{(L_s + L_m)} + 1 \right] i_{ds2} \\ \quad + \frac{L_m V_s (1-c)}{(L_s + L_m)} \end{cases} \tag{22}$$

$$\begin{cases} P_{s1} = V_s i_{qs1} = \frac{V_s L_m}{(L_s + L_m)} (C - 1) i_{qs2} \\ Q_{s1} = \left[\frac{V_s L_m}{(L_{s1} + L_m)} (C - 1) \right] i_{ds2} + \frac{V_s^2}{\omega_s (L_{s1} + L_m)} \left[\frac{L_m C}{L_{s1}} + 1 \right] \end{cases} \quad (23)$$

With:

$$C = \left[\frac{L_{s1} L_m}{(L_r + L_m)(L_{s1} + L_m) - L_m^2} \right] \quad (24)$$

The DSIG diagram in Fig. 5 is derived from the star 2 voltages (v_{2ds} , v_{2qs}) and the star 1 P_s and Q_s (P_{s1} , Q_{s1}) values given by Eqs. (22) and (23), respectively.

The use of the FOC technique in the area of control is accompanied by numerous negatives, as it is greatly affected by the change in the DSIG parameters, and this appears through the rise in fluctuations and the value of current THD, which is undesirable. There are several solutions proposed in the area of control, the most prominent of which was the use of the DPC technique. However, the BC technique is considered one of the most famous of these solutions that can be relied upon due to its high robustness against changing machine parameters. This approach provides very satisfactory results compared to the FOC technique and some other controls, as was explained in the introduction section.

The BC technique

In the area of control, the BC technique is considered a nonlinear approach that has provided impressive results compared to linear strategies and some existing nonlinear controls such as the SMC technique. Its use allows for an important increase in the features of the control system, especially robustness, which makes it one of the best solutions that can be relied upon. The basic principle of the BC technique is to render closed-loop systems equivalent to first-order subsystems in cascade form, which are Lyapunov stable. This ensures robustness and asymptotic global stability⁶⁶. However, it is significant to note that the BC technique here is based on the VC technique theory and is used to control the DSIG. To use the BC strategy, you must know the MM of the DSIG accurately. Also, this approach contains a significant number of gains, as these gains are used to adjust and change the RT.

In this case, reference frame (d-q) control is applied, taking into account the direction of the stator flux⁶⁷:

$$\begin{cases} \phi_{qs1} = 0 \\ \phi_{ds1} = \phi_s = \frac{V_s}{\omega_s} \end{cases} \quad (25)$$

The equations below are the currents derived for star 1 of the stator:

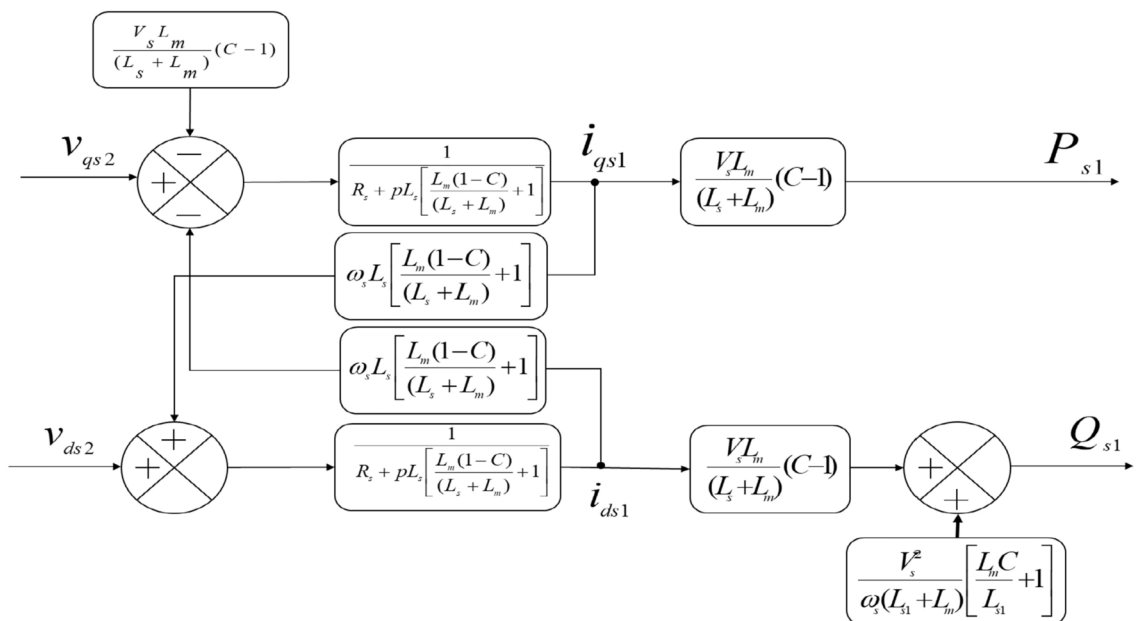


Fig. 5. The DSIG model.

$$\begin{cases} \dot{i}_{ds2} = \frac{di_{ds2}}{dt} = \frac{v_{ds2}}{L_s \left[1 + \frac{L_m(1-C)}{(L_s+L_m)} \right]} - \frac{R_s}{L_s \left[1 + \frac{L_m(1-C)}{(L_s+L_m)} \right]} i_{ds2} - \frac{\omega_s}{C} i_{qs2} \\ \dot{i}_{qs2} = \frac{di_{qs2}}{dt} = \frac{v_{qs2}}{L_s \left[1 + \frac{L_m(1-C)}{(L_s+L_m)} \right]} - \frac{R_s}{L_s \left[1 + \frac{L_m(1-C)}{(L_s+L_m)} \right]} i_{qs2} + \frac{\omega_s}{C} i_{dr} \\ + \frac{V_s}{L_{s1}} + \frac{L_m V_s(1-C)}{L_s - L_m C} \end{cases} \quad (26)$$

The following equations express the relation between the energies and currents of stars 1 and 2:

$$\begin{cases} \dot{i}_{qs2_ref} = \frac{\dot{P}_{s2_ref}}{V_S} \\ \dot{i}_{ds2_ref} = \frac{\dot{Q}_{s2_ref}}{V_S} \end{cases} \quad (27)$$

This controller can be synthesized in two steps. First, the control voltage is determined using Lyapunov functions. Second, the regulator is established in two steps as follows.

First step

Speed loop: e_1 and e_2 represent the errors between the measured variables of the currents i_{qs2} and i_{ds2} and the reference variables i_{qs2_ref} and i_{ds2_ref} , which are determined in this step as follows:

$$\begin{cases} e_1 = i_{qs2_ref} - i_{qs2} \\ e_2 = i_{ds2_ref} - i_{ds2} \end{cases} \quad (28)$$

The derivatives of Eq. (27) are:

$$\begin{cases} \dot{e}_1 = \dot{i}_{qs2_ref} - \dot{i}_{qs2} \\ \dot{e}_2 = \dot{i}_{ds2_ref} - \dot{i}_{ds2} \end{cases} \quad (29)$$

Consider the following Lyapunov candidate function:

$$v = \frac{1}{2} (e_1^2 + e_2^2) \quad (30)$$

To force the Lyapunov function derivative to zero, the errors should be selected as follows:

$$\dot{e}_1 = -k_1 e_1 \text{ and } \dot{e}_2 = -k_2 e_2.$$

After derivation, Eq. (30) becomes:

$$\dot{V}_1 = -k_1 e_1^2 - k_2 e_2^2 < 0 \quad (31)$$

With: $K_1 > 0$ and $K_2 > 0$.

This indicates that our system is globally stable. By replacing the derivatives of the reference currents (I_{dr_ref} and I_{qr_ref}) with their respective values, we obtain the formulation for the derivative errors, given by:

$$\begin{cases} \dot{e}_1 = \frac{\dot{P}_{s2_ref}}{V_S} - \frac{v_{qs2}}{L_s \left[1 + \frac{L_m(1-C)}{(L_s+L_m)} \right]} + \frac{R_s}{L_s \left[1 + \frac{L_m(1-C)}{(L_s+L_m)} \right]} i_{qs2} \\ - \frac{\omega_s}{C} i_{dr} - \frac{V_s}{L_{s1}} - \frac{L_m V_s(1-C)}{L_s - L_m C} \\ \dot{e}_2 = \frac{\dot{Q}_{s2_ref}}{V_S} - \frac{v_{ds2}}{L_s \left[1 + \frac{L_m(1-C)}{(L_s+L_m)} \right]} + \frac{R_s}{L_s \left[1 + \frac{L_m(1-C)}{(L_s+L_m)} \right]} i_{ds2} \\ + \frac{\omega_s}{C} i_{qs2} \end{cases} \quad (32)$$

Step two

In this step, our goal is to calculate the control voltage. First, all faults are identified in star 2 for the stator current components and their references.

$$\left\{ \begin{array}{l} -k_1 e_1 = \frac{\dot{P}_{s2_ref}}{V_s} - \frac{v_{qs2}}{L_s \left[1 + \frac{L_m(1-C)}{(L_s+L_m)} \right]} + \frac{R_s}{L_s \left[1 + \frac{L_m(1-C)}{(L_s+L_m)} \right]} i_{qs2} \\ \quad - \frac{\omega_s}{C} i_{ds2} - \frac{V_s}{L_{s1}} - \frac{L_m V_s (1-C)}{L_s - L_m C} \\ -k_2 e_2 = \frac{\dot{Q}_{s2_ref}}{V_s} - \frac{v_{ds2}}{L_s \left[1 + \frac{L_m(1-C)}{(L_s+L_m)} \right]} + \frac{R_s}{L_s \left[1 + \frac{L_m(1-C)}{(L_s+L_m)} \right]} i_{ds2} \\ \quad + \frac{\omega_s}{C} i_{qs2} \end{array} \right. \quad (33)$$

Finally, the selection of the control law is as follows:

$$\left\{ \begin{array}{l} v_{qs2} = \left(\frac{\dot{P}_{s2_ref}}{V_s} + k_1 e_1 \right) L_s \left[1 + \frac{L_m(1-C)}{(L_s+L_m)} \right] + R_s i_{qs2} \\ \quad - \left(\frac{\omega_s}{C} i_{ds2} + \frac{V_s}{L_{s1}} + \frac{L_m V_s (1-C)}{L_s - L_m C} \right) L_s \left[1 + \frac{L_m(1-C)}{(L_s+L_m)} \right] \\ v_{ds2} = \left(\frac{\dot{Q}_{s2_ref}}{V_s} + k_2 e_2 \right) L_s \left[1 + \frac{L_m(1-C)}{(L_s+L_m)} \right] + R_s i_{ds2} \\ \quad + \frac{\omega_s}{C} \left[1 + \frac{L_m(1-C)}{(L_s+L_m)} \right] i_{qs2} \end{array} \right. \quad (34)$$

The parameters of the BC approach of DSIG can be calculated using the method of experimentation and simulation or using smart strategies, as was proposed in this research study to use the smart strategy for this purpose.

Using the BC approach to control the power of a DSIG creates several undesirable problems. The most prominent of these defects is the decrease in durability in the event of a change in the machine parameters. Power quality and current are among the most prominent of these defects as well. These defects can be attributed to the gain values of the BC approach. In the next section, an effective solution is proposed to overcome the drawbacks of the BC approach. This proposed solution gives satisfactory results and is characterized by high performance.

Proposed BC-ALO technique

In this section, the solution proposed in this paper for power control of DSIG is discussed in detail. The proposed solution is based on the use of the strategy detailed in section four. This proposed strategy is a modification and development of the BC approach of the DSIG. Using this proposed solution allows for improving power quality and significantly reducing the THD of current. The proposed solution is based on the use of the ALO algorithm to calculate the gain values of the BC approach. Therefore, the proposed approach is characterized by high robustness, great efficiency, and outstanding performance.

Mostly, experimentation and simulation method is used to calculate gain values. Using this strategy does not always give satisfactory results in terms of power quality and THD of current. To obtain satisfactory results and system stability, the parameters of the proposed approach to power control must have positive values. Therefore, to obtain outstanding performance, the parameters must be chosen correctly, as smart strategies remain the optimal choice. Therefore, this study proposes an approach based on the ALO technique for offline parameter selection in this paper. The use of the ALO strategy ensures optimal values of BC technology parameters and thus high quality of current and power. Figure 6 represents the proposed approach based on the ALO strategy used for capacity control in this paper. This figure gives a clear picture of the proposed strategy, as this proposed strategy is applied to one star only, and the other star is connected to the network directly without an intermediary.

Notably, the ALO technique is employed offline to determine the optimal parameter values for the BC technique. As shown in Fig. 6, the control performance is subject to fluctuations that depend on the tuning parameters (K_1 and K_2). These tuning parameters are based on the error of the direct stator (star 2) tow current component I_{2sd} related to the Q_s of the DSIG and the error of the quadrature stator (star 2) current component I_{2sq} related to P_s .

This designed BC-ALO technique aims to generate VRRVs based on a power error. In this designed BC-ALO technique, the PWM technique is used to create the necessary operating pulses for the DSIG inverter. The BC-ALO technique is applied to both the DSIG inverter and the grid inverter, which makes the designed BC-ALO technique system very efficient. The MPPT technique is used to conclude the reference value of P_s , which allows obtaining a maximum value of power.

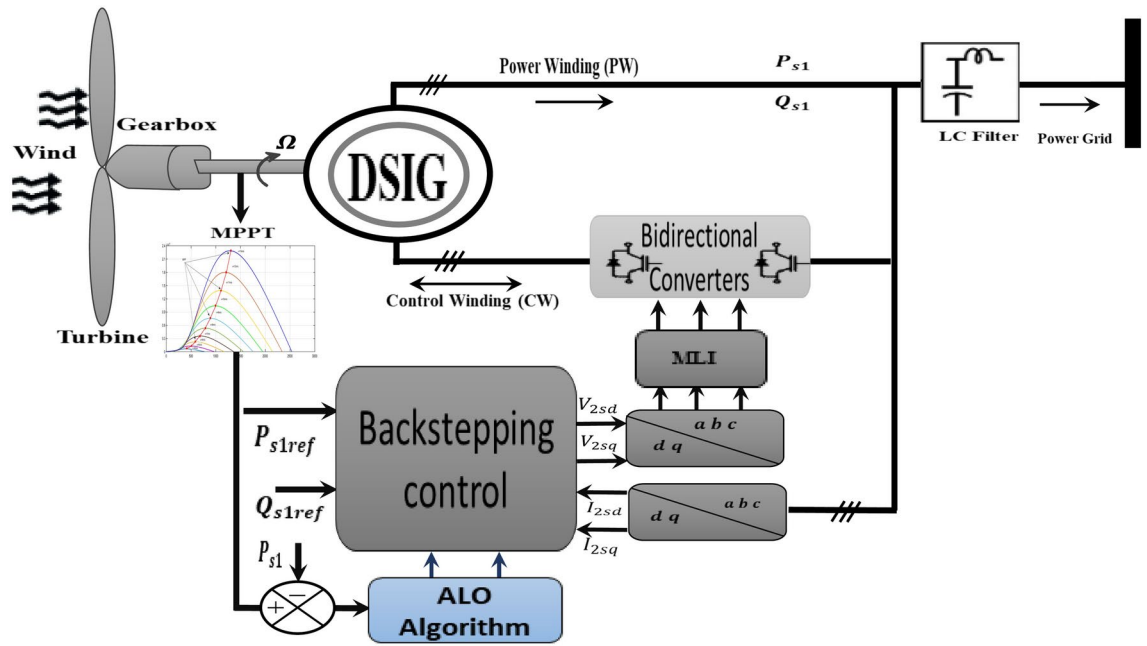


Fig. 6. BC-ALO approach for DSIG-WT.

As is known, the values and number of gains play a major role in obtaining a fast DR and high power quality for any control. Therefore, it is necessary to use a well-organized method or strategy to obtain these values. Several strategies can be used to determine payoff values, such as genetic algorithms, the GWO technique, and the particle swarm optimization approach. However, the ALO strategy is considered one of the most prominent strategies that can be relied upon to calculate the gains of control strategies, regardless of their degree of complexity. ALO is easy to use.

The ALO technique, presented in Ref.⁶⁸, is a population-based optimization technique that emulates the hunting behavior of ant lions found in nature. Ant lions construct inverted cone-shaped pits in sand using their massive jaws⁶⁹ to trap their prey, typically ants. The ALO approach works by representing each candidate solution as an ant lion, and the position of each ant lion is updated based on the fitness of its solution and its proximity to other ant lions. The algorithm incorporates randomization to prevent becoming trapped at local optima, enabling full exploration of the search space. After capturing its prey, an ant lion cleans out the pit for another hunt⁶⁹. The ALO approach is an algorithm that differs from other approaches, such as the genetic algorithm, as this approach is considered new and little used. The ALO approach has several advantages, including fast convergence speed, high precision, ease, scalable, flexibility, and a great balance between exploration and exploitation⁷⁰.

The ALO approach (Fig. 7) parameters employed in this study for tuning the BC technique parameters consist of 50 ant lions and a maximum of 100 iterations. Initially, the ALO is executed offline to identify the optimal BC parameters (K1 and K2). The first generation is stochastically generated, with a dimensionality of 2 (K1 and K2) derived from the initial ALO approach parameters. Table 1 presents the optimal parameters for each iteration along with their corresponding fitness values, which are crucial for evaluating the objective function. Additionally, Figs. 8 and 9 illustrate the variations in the fitness function and the optimal parameters (K1 and K2) obtained through the ALO approach during the simulation. From Figs. 8 and 9, it is evident that the best fitness value achieved is evaluated to be 1.246e+06, with optimal gains of k1 = 3.7772e+03 and K2 = 4.3250e+03. These optimized parameters demonstrate convergence over approximately 100 iterations, highlighting the efficacy of the ALO approach in efficiently exploring optimal BC approach parameters.

The tuning parameters K_1 and K_2 , as illustrated in Fig. 7, are associated with the error of the stator WC quadrature current component i_{2sq} related to P_{s1} and the error of the direct current component i_{2sd} associated with Q_{s1} of the DSIG. These factors influence the variation in command performance. The controller's efficacy was evaluated using two performance metrics: the ITAE (Integral time absolute error) and the ITSE (Integral time square error). The definitions of the ITAE and ITSE indices are as follows⁷¹:

$$ITSE = \int_0^{\infty} t \cdot e(t)^2 dt, \tag{35}$$

$$ITAE = \int_0^{\infty} t \cdot |e(t)| dt. \tag{36}$$

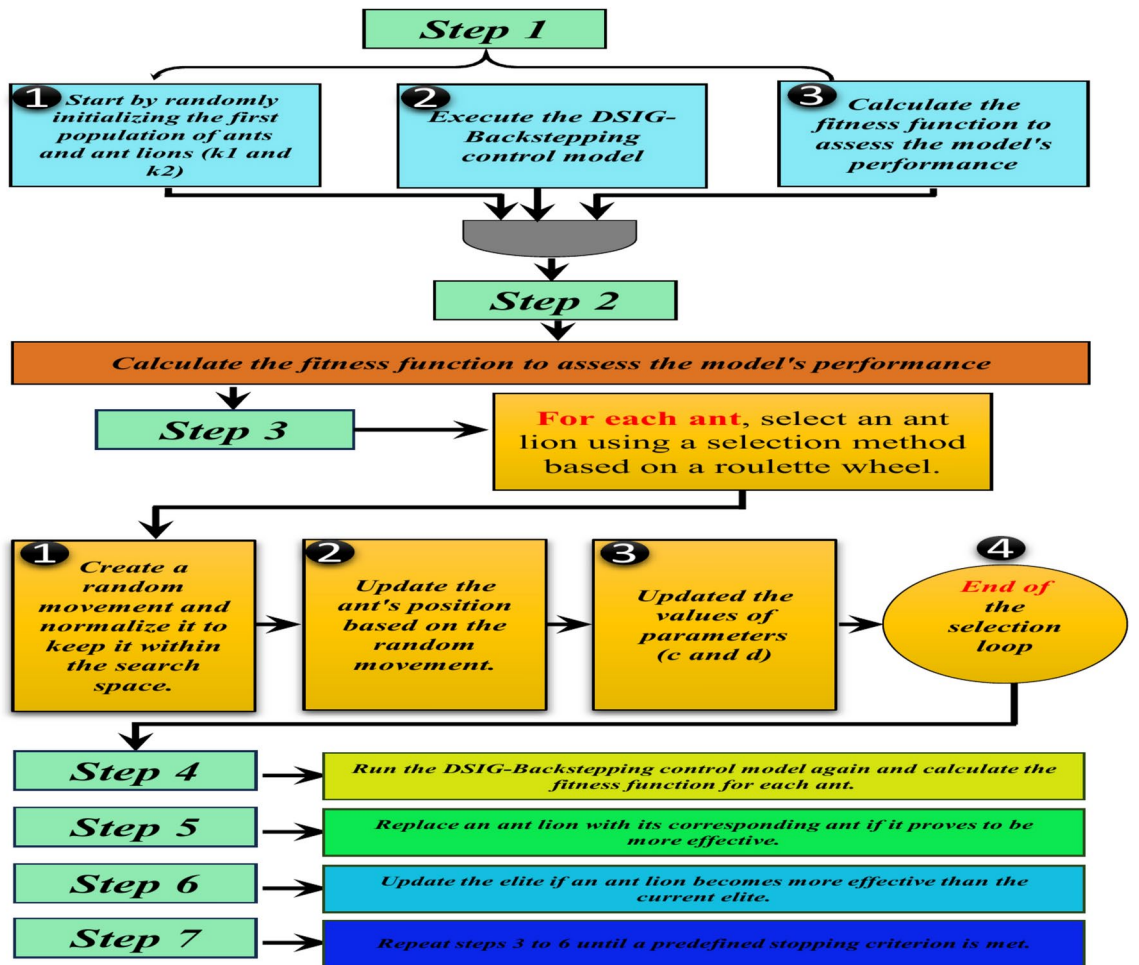


Fig. 7. Pseudo-code of the BC-ALO for the DSIG.

Iteration no.	Optimal parameters	Fitness values
1	K1(1, 1) = 3.0635 e+003	1.290e+006
	K2 (1, 2) = 7.7103 e+003	
15	K1(15, 1) = 6.5325 e+003	1.281e+006
	K2 (15, 2) = 7.3842 e+003	
20	K1(20, 1) = 4.0796 e+003	1.271e+006
	K2 (20, 2) = 4.4009 e+003	
30	K1(30, 1) = 3.7174 e+003	1.265e+006
	K2 (30, 2) = 3.9126 e+003	
50	K1(50, 1) = 4.0349 e+003	1.260e+006
	K2 (50, 2) = 4.1494 e+003	
80	K1(80, 1) = 3.8794 e+003	1.251e+006
	K2 (80, 2) = 4.3508 e+003	
100	K1(100, 1) = 3.7772 e+003	1.246e+006
	K2 (100, 2) = 4.3250 e+003	

Table 1. Fitness value of each ALO technique.

To study the stability of the proposed approach, the Bode curve or Lyapunov's theory can be used. Lyapunov's theory is based on derivation calculations, which makes it complex and requires knowledge of the MM of the studied system precisely. In the case of complex systems, the use of Lyapunov's theory becomes impossible due to the presence of large calculations. However, the Bode curve is considered one of the most prominent methods that can be relied upon to prove the stability of any control strategy. Compared to Lyapunov's theory,

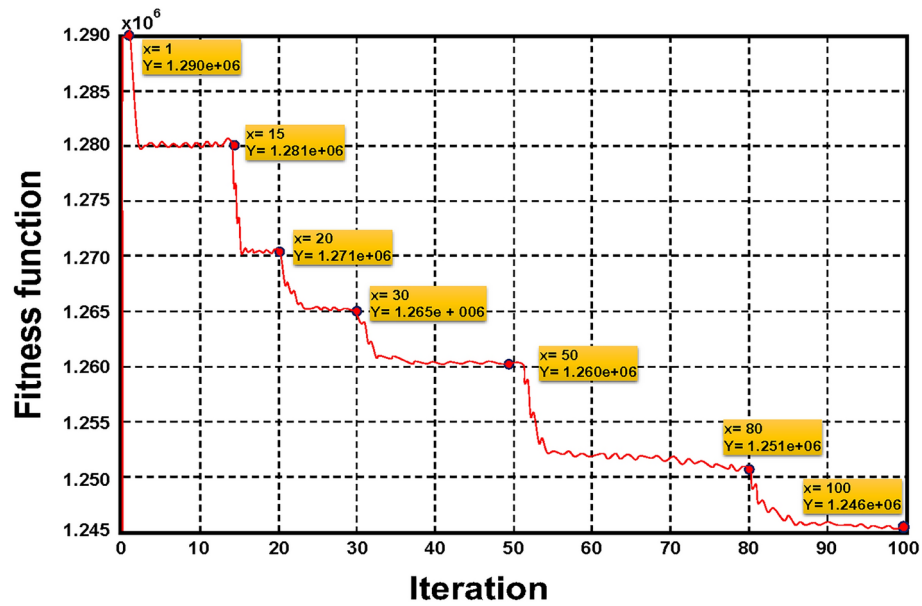


Fig. 8. Fitness function variation during simulation.

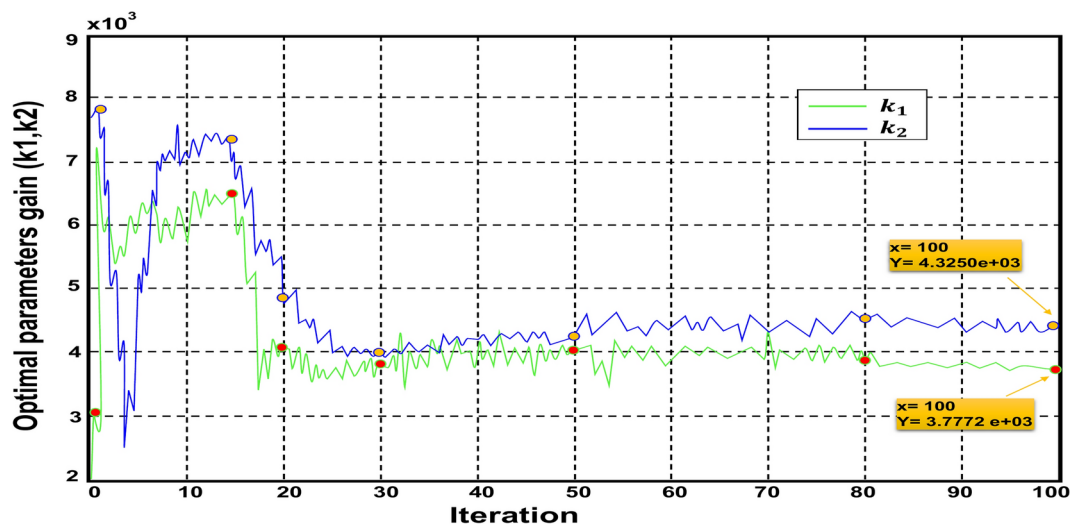


Fig. 9. Variations in the optimal parameters during simulation.

the Bode curve is a method that does not require complex calculations, as MATLAB is relied upon to extract the Bode curve. Therefore, the Bode curve method is a graphical method. Using the Bode curve does not require knowledge of the MM of the carefully studied system, which makes it easy and quick to prove the stability of control systems.

Due to the ease of using the Bode curve, it was relied upon in this paper to prove the stability of the BC-ALO approach of DSIG. Figure 10 represents the Bode curve for the two controllers used in this paper. Using the Bode curve, phase (deg) and Magnitude (dB) are extracted for two controls. Using these two values, the stability of the proposed approach can be proven. From Fig. 10, it is noted that the two approaches have almost the same shape as the Bode curve change, with the proposed approach having an advantage over the traditional BC approach. Also, it is noted that the values of both Phase (deg) and Magnitude (dB) take negative values in the case of the two controls. The phase value changes from 0 to -90 degrees for two controls, and the Magnitude (dB) value changes from -5 to -40 dB for the traditional control. In the case of the proposed control, the Magnitude (dB) value changes from -7 to -40 dB. Table 2 represents numerical values extracted from the Bode curve for two controls.

The comparative analysis of the traditional BC technique and BC-ALO approach reveals significant enhancements in both stability margins and DR. The gain margin improved by 40.23%, increasing from 15.30 to 25.60 dB, indicating a substantially higher tolerance to gain variations before instability. Concurrently, the

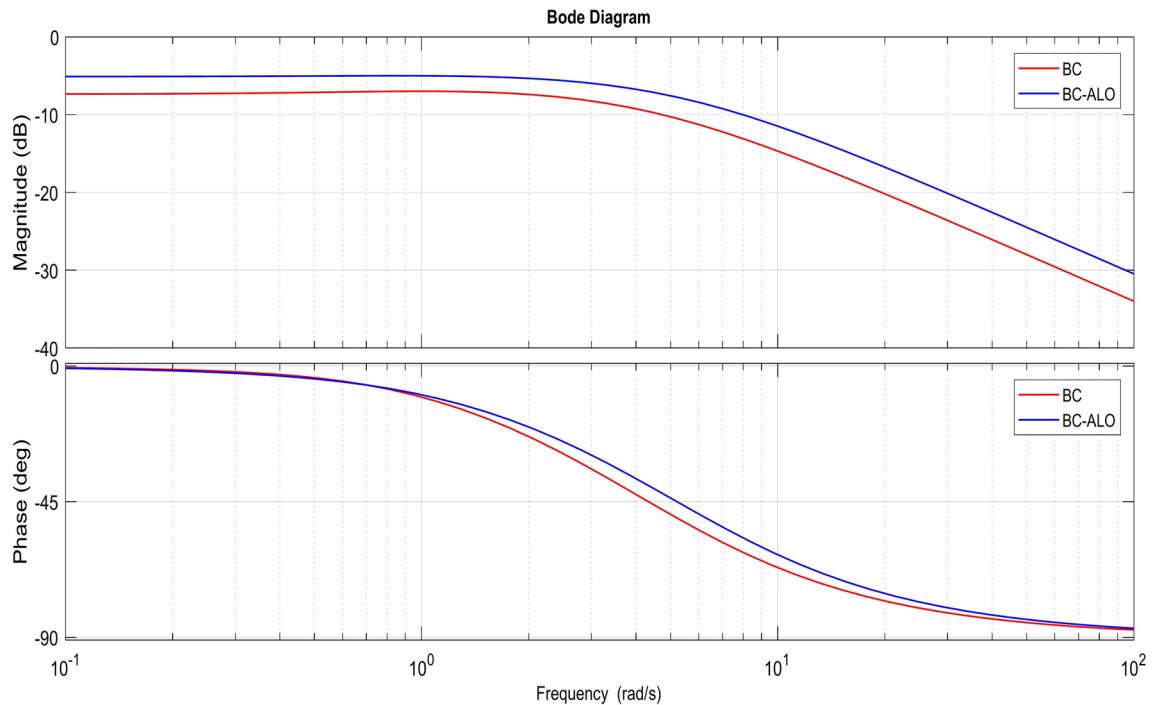


Fig. 10. Bode curve for two controllers.

Criterion	BC	BC-ALO	Ratios (%)
Gain margin (dB)	15.30	25.60	40.23
Phase margin (deg)	45.50	65.20	30.21
Crossover frequency (rad/s)	3.8	5.2 rad/s	26.92
Resonance peak (dB)	3.5 dB	1.8 dB	48.57

Table 2. Budd curve characteristics for two controllers.

phase margin exhibited a 30.21% improvement, rising from 45.50 to 65.20 deg, which underscores the optimized system's robustness against phase delays and transient oscillations. The crossover frequency shifted from 3.8 to 5.2 rad/s, reflecting a faster DR while maintaining closed-loop stability. Moreover, the resonance peak value was estimated at 3.5 dB and 1.8 dB for both the conventional BC strategy and the proposed approach, respectively. These values indicate that the proposed approach reduces the value of the resonance peak significantly compared to the traditional BC approach. This reduction was estimated at 48.57%. This percentage indicates the effectiveness of the proposed approach in reducing the severity of the resonance peak, which is positive. These improvements are attributed to the ALO algorithm's ability to refine control parameters, achieving an optimal trade-off between stability and performance. The results conclusively validate the superiority of the BC-ALO approach in enhancing system robustness and dynamic precision for applications requiring high reliability under parametric uncertainties and external disturbances.

Results

To verify the validity, efficiency, and performance of the approach proposed in this paper, the MATLAB environment is used. In this work, a DSIG with a capacity of 1.5 MW was used. Also, two different wind speed profiles were used to study the effectiveness of the designed approach in improving power quality and reducing the THD of current. The results of the proposed approach are compared with the BC strategy. The turbine parameters used in this work are as follows: Gearbox=90, hub height=85 m, number of blades=3, radius of the blades=60, and friction coefficient=0.24. On the other hand, the generator parameters used in this paper are as follows: $J=30 \text{ kg m}^2$, $f=2.5 \text{ N m s/rd}$, $P_n=1.5 \text{ MW}$, $V=400 \text{ V}$, $f_s=50 \text{ Hz}$, number of pole pairs=2, rotor resistance=0.007 Ω , stator resistance= $r_1=r_2=0.008 \Omega$, $L_r=0.067 \text{ mH}$, and $L_1=L_2=0.134 \text{ mH}$.

In the next subsection, a variable wind speed is used to test the efficiency and effectiveness of the proposed approach compared to the BC approach. The necessary numerical values and graphical results are extracted to compare the results and show the superiority of the designed approach in improving the system features.

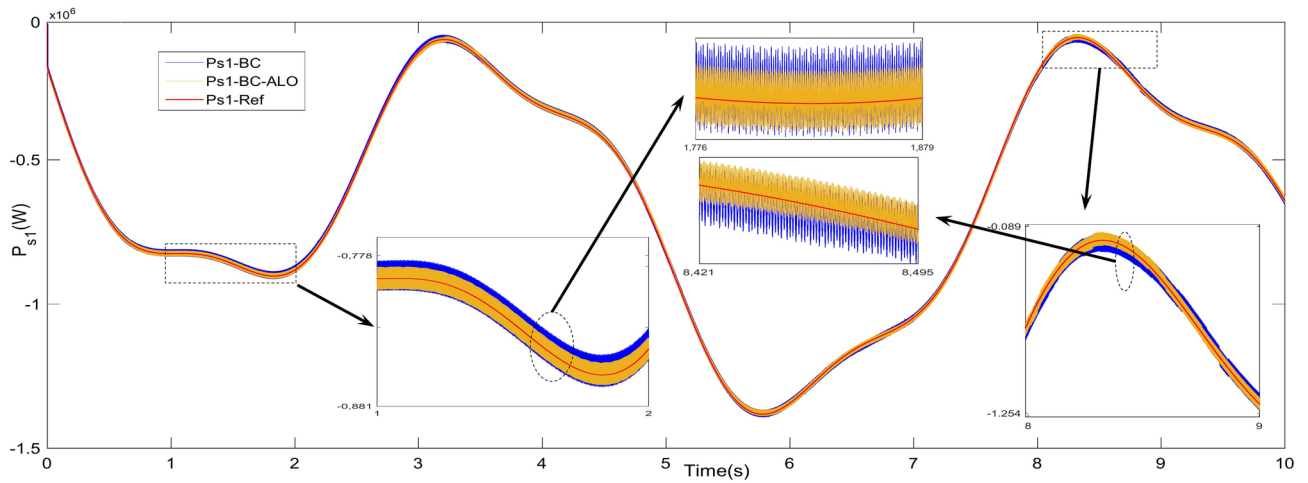


Fig. 11. Active power of a generator in the case of two techniques (First test).

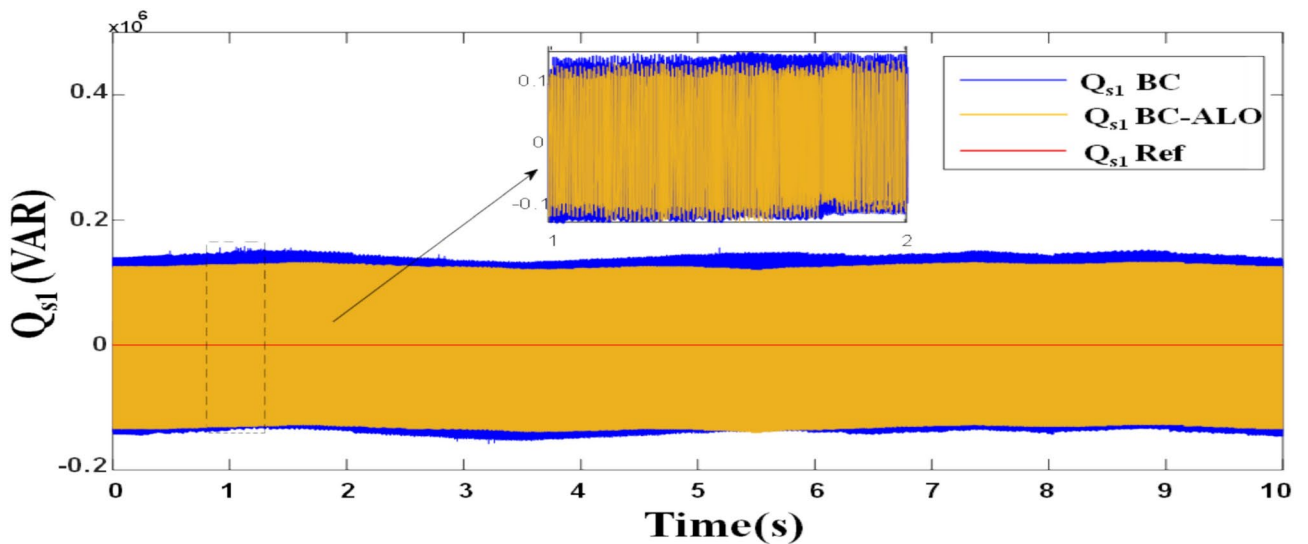


Fig. 12. Reactive power of a generator in the case of two approaches (First test).

First test

In this test, a variable WS is used to test the behavior of the proposed approach. Figures 11 and 12 depict the simulation results of two control techniques, the BC technique, and the BC-ALO approach, applied to a tracer scenario involving P_s and Q_s , along with their references. The simulations were conducted using the MPPT and unity power factor under fluctuating WSs. The suggested BC-ALO technique shows impressive reference tracking ability and notably reduces P_s and Q_s ripples in the first-star stator compared to the BC technique, which lacks an optimization algorithm.

The change in P_s follows a change in WS. As the WS increases, the value of P_s increases, and vice versa. However, the Q_s do not change according to the change in WS, as its value remains constant and equal to zero.

In Fig. 13, the DC bus link for the two approaches is shown. This tension follows the reference well, as it takes a value of 1130 V for both controls, with an exceedance of the limit value in the case of using the BC technique. Also, the BC-ALO technique provided a better RT than the BC technique for the DC bus link, which is a good thing. Moreover, as illustrated in Fig. 13, WS fluctuations have a distinct effect on the voltage of the DC bus link. This impact is particularly pronounced in the BC strategy, where multiple distortions and harmonics are observed, in contrast to the optimized BC-ALO approach. Consequently, it can be inferred that the proposed system operates with enhanced precision and stability, leading to improved overall system efficiency.

The current THD in this test for the control scheme is represented in Fig. 14a,b notably; the THD was 1.46% and 1.03% for both the BC approach and the BC-ALO technique, respectively. Therefore, the BC-ALO technique significantly minimized the THD, and the minimization ratio was estimated at 29.45%, indicating that the current quality is better in the case of the designed BC-ALO approach than in the BC technique. Moreover, the amplitude of the fundamental signal (FS) was 1283 A for the BC technique and 1292 A for the proposed

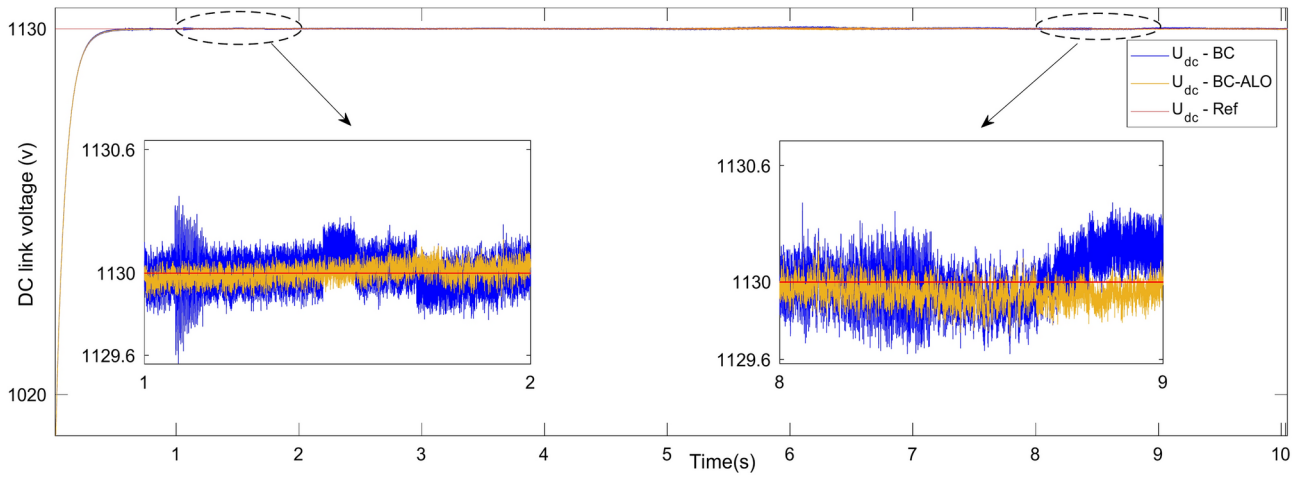


Fig. 13. DC link voltage of the DSIG.

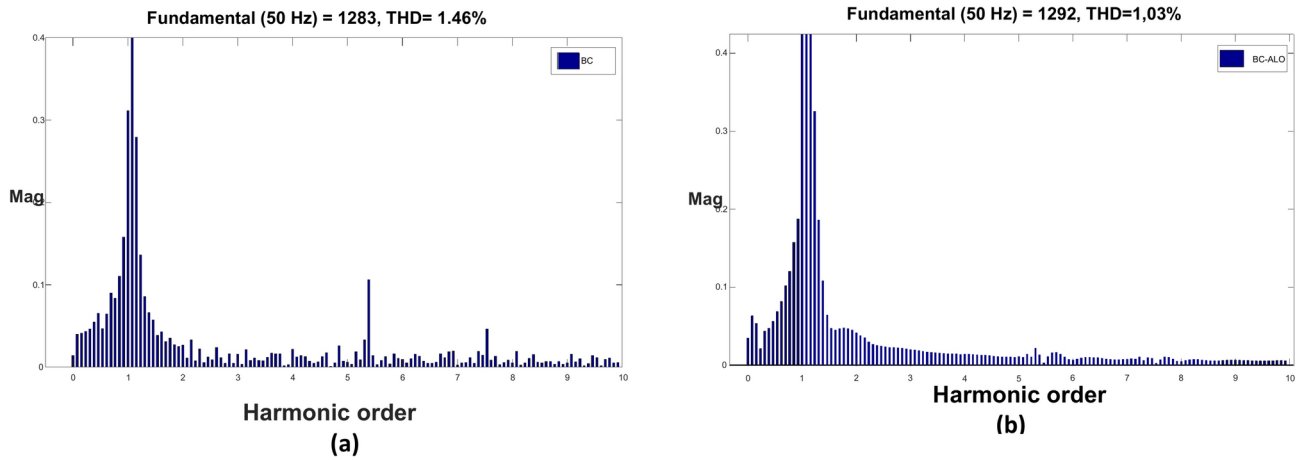


Fig. 14. THD of the current GRID ($i_{s_{ig}}$) in the first test: (a) BC and (b) BC-ALO.

Control performance		BC $K_1 = 8.32e+003$ $K_2 = 8.32e+003$	BC-ALO $K_1 = 3.32721e+003$ $K_2 = 4.72501e+003$	Ratios (%)
P_s	ITSE	2.324e+008	2.132e+008	8.26
	ITAE	1.452e+004	8645	40.46
	Overshoot	2.3265	Negligible	100
	RT (ms)	1.66	1.65	0.60
Q_s (VAR)	Overshoot	5.3265	Negligible	100
	RT (ms)	58.46	1.37	97.65
V_{dc} ripples (V)		3.06845	1.1256	63.31
THD (%)		1.46	1.03	29.45

Table 3. BC technique performance for a DSIG without and with ALO technique.

BC-ALO technique. The proposed BC-ALO technique gave greater amplitude to the FS (50 Hz) than the BC technique, as this augment was estimated at a rate of 0.69%. Accordingly, the BC-ALO technique has a greater scope than the BC technique because this feature is highly important and makes the BC-ALO technique superior for improving the features of power systems and overcoming the defects and cons of conventional techniques.

Based on the data in Table 3, it can be concluded that the BC-ALO approach outperforms the BC technique in terms of RT and the absence of static error, showing a small overshoot of the DC bus voltage. These numerical values indicate the advantage of the BC-ALO technique over the BC technique, making it an appropriate

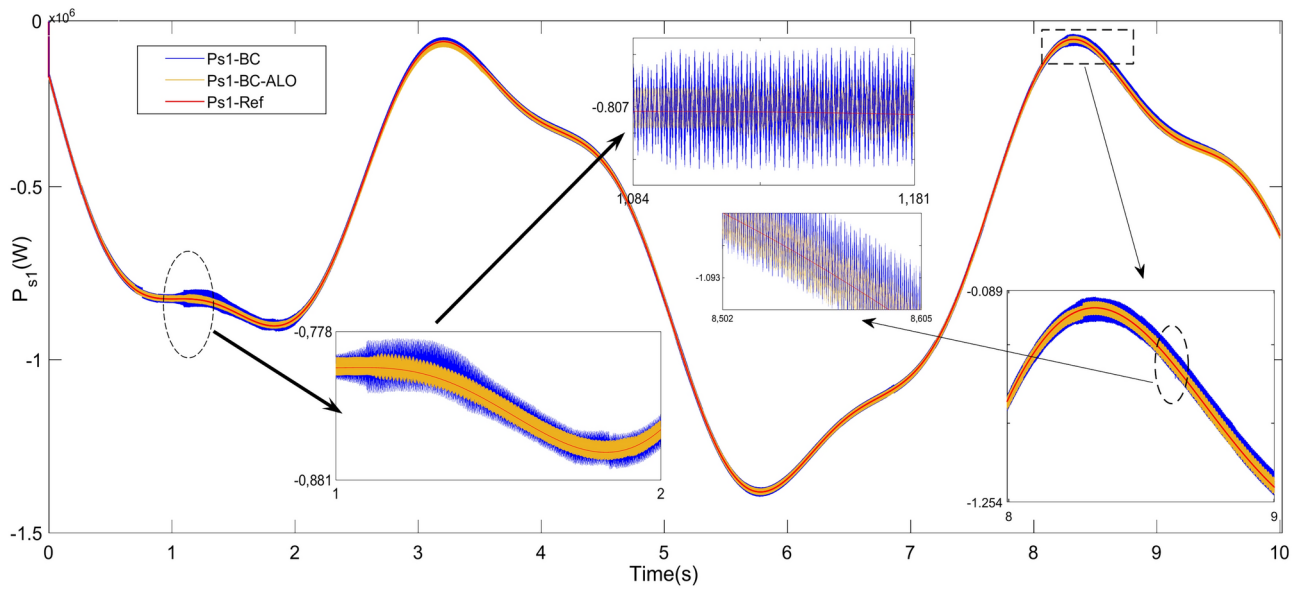


Fig. 15. Active power of a generator in the case of two strategies (Second test).

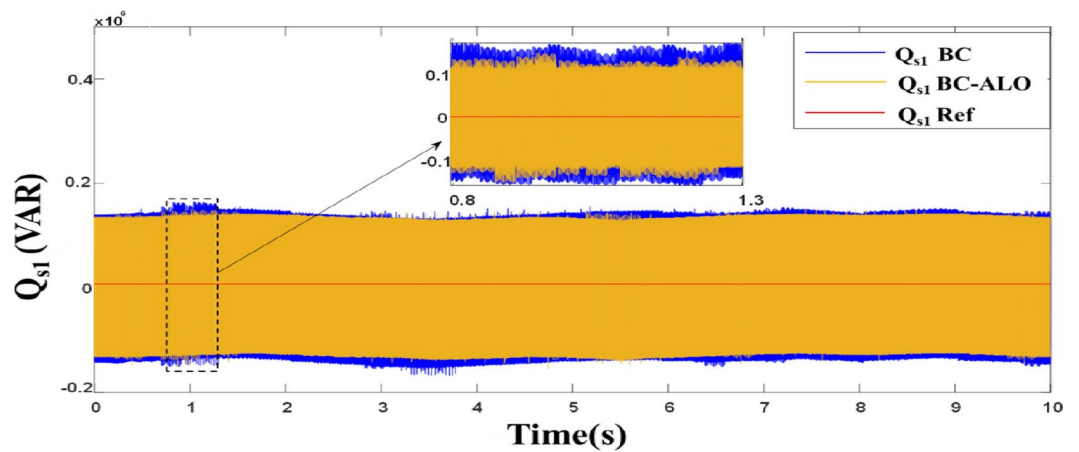


Fig. 16. Reactive power with parameter variations based on two presented control schemes.

solution in the future in the area of control. The advantage of this strategy is confirmed in the second test in terms of changing the DSIG parameters. In the next section, the extent to which this BC-ALO technique is affected by changing DSIG parameters compared to the BC technique is assessed. Based on the numerical values presented in Table 3, the BC-ALO approach provided numerical values for overshoot of Q_s , V_{dc} ripples, RT of P_s , and ITAE and ITSE of P_s that are much lower than the BC technique, which indicates the advantage of this approach in improving the features of the control system. The BC-ALO technique minimized the value of the voltage line ripples compared to the BC technique by an estimated percentage of 63.31%. Also, the overshoot of Q_s compared to the BC technique has been reduced by 100%. The RT for Q_s was 58.46 ms and 1.37 ms for both the BC technique and the proposed BC-ALO technique, respectively. From these values, the BC-ALO technique provided a much lower RT than the BC technique, as this reduction was estimated at 97.65%.

The proposed BC-ALO technique reduced the values of ITSE, overshoot, ITAE, and RT of P_s by percentages estimated at 8.26%, 100%, 40.46%, and 0.60% compared to the BC technique. These calculated ratios make the BC-ALO technique a promising solution in the area of control and highlight the importance of using the ALO strategy in the area of control.

Second test

A robustness test was performed, and it involved modifying the rotor resistance R_r and the stator inductances L_s of the DSIG. Despite regulators theoretically guaranteeing fixed values, these parameters can fluctuate due to various physical phenomena. Figures 15, 16 and 17 depict the variations in P_s and Q_s and the DC bus link voltage of the DSIG, respectively, when the rotor resistance R_r and stator inductances are adjusted by 100% at 1 s.

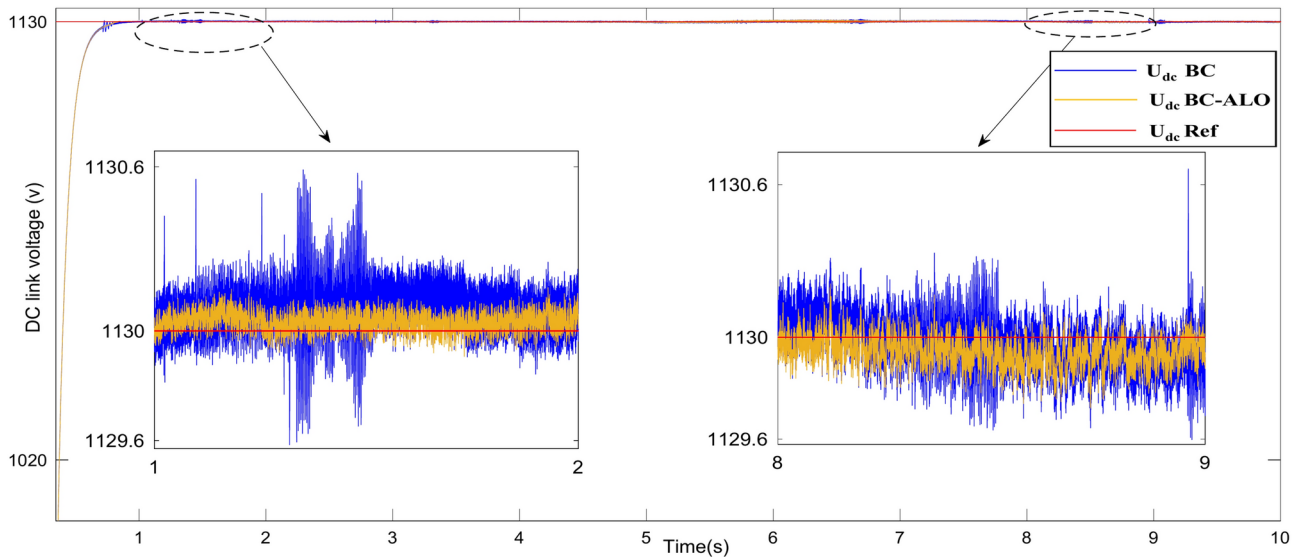


Fig. 17. DC link voltage of the DSIG (Second test).

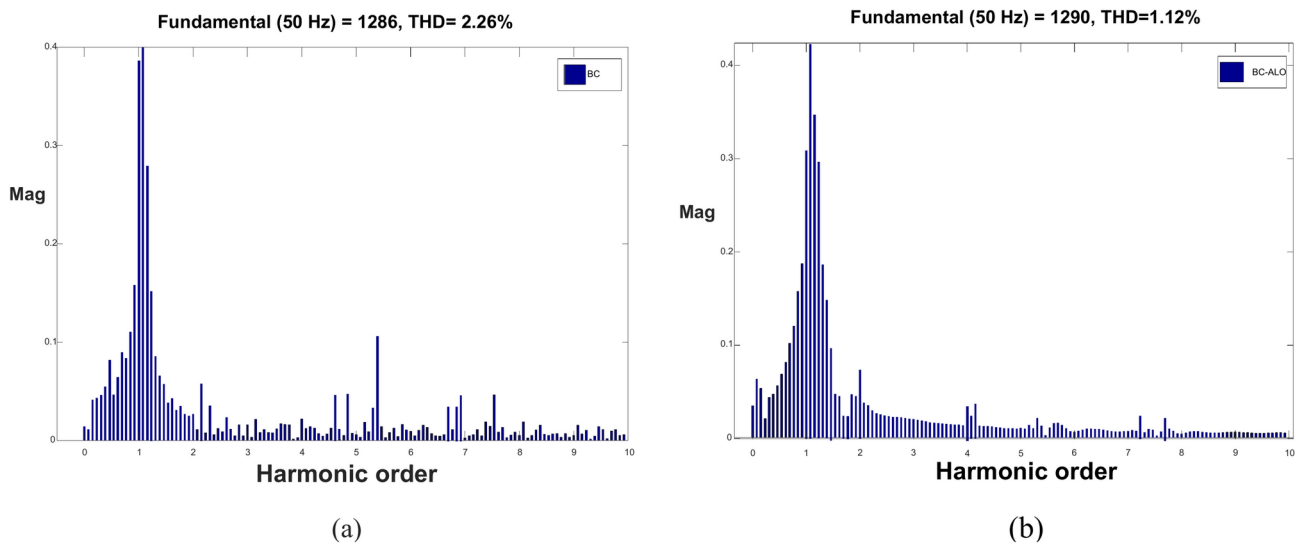


Fig. 18. THD of the current grid ($i_{s_{ig}}$) in the test 2: (a) BC and (b) BC-ALO.

Remarkably, these parameter changes have little impact on DSIG performance due to the compensatory effects of the BC-ALO controllers. These controllers ensure accurate reference tracking and maintain stability even in the face of parameter fluctuations. In contrast, conventional unoptimized control techniques exhibit deficiencies in precise reference tracking, thereby inducing distortions and harmonics.

P_s changes according to the variations in WS, and Q_s are not affected by the WS and remain constant and equal to 0 VAR. The DC link voltage is fixed despite the changes in the DSIG parameters and WS, with a value of 1130 V. Moreover, the ripples of both DC link voltages, P_s and Q_s , are lower when using the BC-ALO technique than when using the BC strategy.

The current THD in this test of the control scheme is represented in Fig. 18a,b. The THDs for the BC technique and BC-ALO approach are 2.26% and 1.12%, respectively. Compared with the BC technique, the BC-ALO strategy notably decreases the THD by 50.44%, indicating enhanced current quality. Additionally, the BC-ALO approach provides a larger amplitude for the FS (50 Hz) than the amplitude provided by the traditional approach, as the amplitudes are estimated at 1286 A and 1290 A for the BC approach and BC-ALO technique, respectively. The BC-ALO technique excels in increasing the ranges of properties for the power system, providing a promising solution to defeat the cons of the BC technique.

The numerical results of this test are listed in Table 4. Based on the data presented in Table 4, the BC-ALO technique gave better numerical values than the BC technique despite the change in system parameters in terms of RT and the values of overshoot, ITAE, and ITSE of P_s . Also, in terms of the values of both DC bus voltage ripples

Control performances		BC $K_1 = 8.32e + 003$ $K_2 = 8.32e + 003$	BC-ALO $K_1 = 3.26341e + 003$ $K_2 = 3.93206e + 003$	Ratios (%)
P_s (W)	ITSE	2.624e + 008	2.202e + 008	16.08
	ITAE	1.352e + 004	9645	28.66
	Overshoot	2.7313	Negligible	100
	Response (ms)	4.36	2.03	53.44
Q_s (VAR)	Overshoot	9.5228	Negligible	100
	Response (ms)	98.46	2.18	97.78
V_{dc} ripples		7.06845	2.0256	71.38
THD (%)		2.62	1.12	57.25

Table 4. Performance of both techniques (second test).

		Techniques	
		BC	BC-ALO
THD of the current	First test	1.46	1.03
	Second test	2.26	1.12
	Second test–first test	0.80	0.09
	Ratios	35.39%	8.03%
Amplitude of the FS of the current (A)	First test	1283	1292
	Second test	1286	1290
	Second test–first test	3	–2
	Ratios	0.23%	–0.15%

Table 5. Changes in the THD and amplitude of the FS during the first and second tests.

and Q_s overshoot. Accordingly, the BC-ALO technique reduced the values of RT, overshoot, ITSE, and ITAE of P_s by percentages estimated at 53.44%, 100%, 28.66%, and 16.08%, respectively, compared to the BC technique. The overshoot value of Q_s was also reduced by an estimated 100% compared to the BC technique. The RT for Q_s was 98.46 ms and 2.18 ms for both the BC technique and the BC-ALO technique, respectively. Accordingly, the BC-ALO technique significantly reduced the RT of Q_s compared to the BC strategy, as this minimization was estimated at 97.78%. The DC link voltage ripples were 7.06845 V and 2.0256 V for the BC technique and the BC-ALO technique, respectively. These values indicate that the DC link voltage fluctuations are lower when using the BC-ALO technique compared to the BC technique. So, the suggested BC-ALO technique reduced the DC link voltage ripples by an estimated 71.38% compared to the BC technique. So these percentages show the advantage of the BC-ALO technique and the extent of its high ability to improve the system features despite changing parameters, which is a good thing.

Using the numerical results of the two tests in terms of the amplitude of the FS (50 Hz) and the THD, the changes in these two values and the extent of their influence in the two tests are studied, as shown in Table 5. Table 5 shows that the THD augmented significantly in the second test compared to that in the first test, which indicates that the THD is affected by changes in the DSIG parameters, and this increase was greater in the case of the BC approach than for the BC-ALO approach. This effect was estimated at 35.39% and 8.03% for the BC approach and BC-ALO approach, respectively. Therefore, the BC-ALO approach is less affected in terms of the THD by changing the DSIG parameters; consequently, the current quality is better if the BC-ALO approach is used than if the BC approach is used. In Table 5, the change in the amplitude of the FS (50 Hz) for the two control schemes is presented. It is noted that this amplitude was affected by the changes in DSIG parameters, and the values changed in the second test compared to those in the first test. With the BC approach, the amplitude augmented in the second test compared to that in the first test, and this augment was estimated to be 0.23%. With the BC-ALO strategy, the amplitude decreased in the second test compared to that in the first test, and this decrease was estimated to be 0.15%. Therefore, the amplitude and THD were affected by changes in the DSIG parameters, and this effect was less pronounced when the BC-ALO strategy was used than when the BC approach was used.

Third test

In this test, the efficiency of the BC-ALO approach is studied using another form of WS change, as the form of WS change used differs from the form used in the first test. In this test, the efficacy, robustness, and efficiency of the BC-ALO approach are studied compared to the BC approach using the WS in steps, where the shape of the change in this speed is represented in Fig. 19.

The results of this test are represented in Figs. 20, 21, 22, 23 and 24. In Table 6 the numerical results of this test are listed.

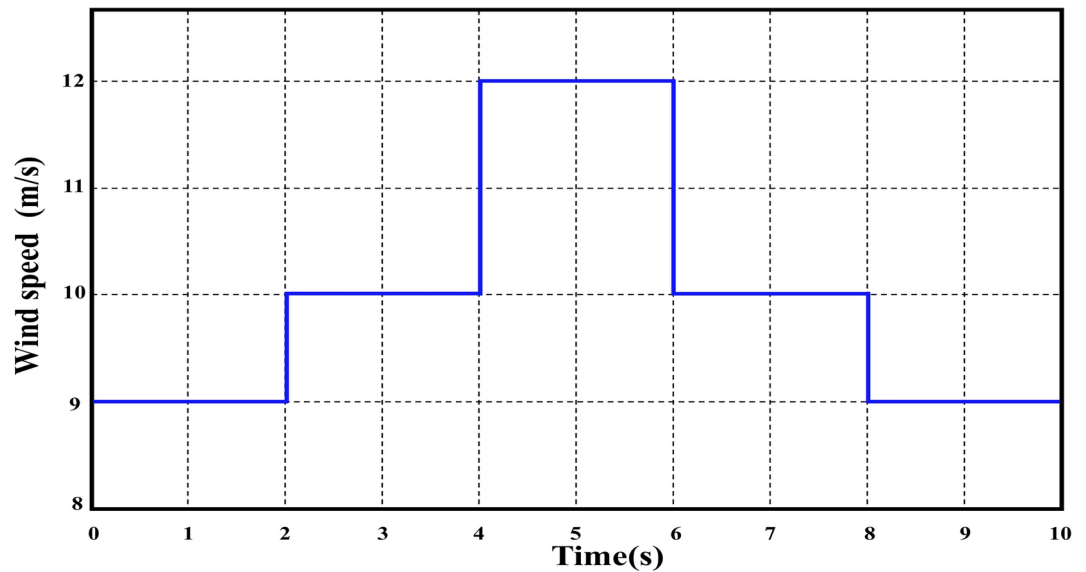


Fig. 19. Steps WS profile.

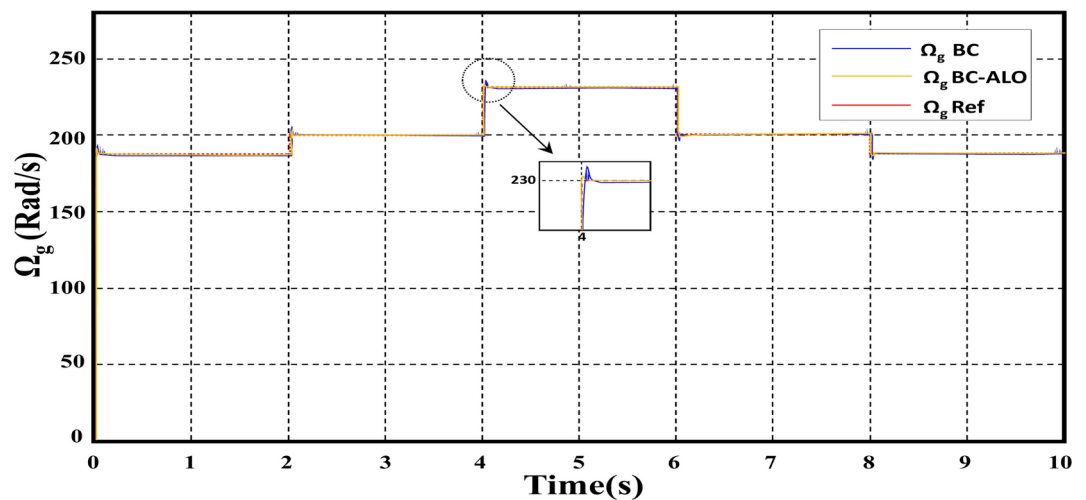


Fig. 20. The shape of the generator speed change in the case of two controls (Third test).

Figure 20 represents the change in the speed of the DSIG as a function of time, as the change in this speed is the same as the change in the WS for the two controls. It is noted that there is an exceedance of the limit value of speed, and this exceedance is large in the case of using the BC approach compared to the BC-ALO approach. Also, the speed of the DSIG is greater when the WS is greater and vice versa, wherein the time ranges from 4 to 6 s the speeds of the DSIG take their largest value.

In Fig. 21, the change in P_s of the two approaches is shown. This power changes according to the change in WS, as it decreases and increases with a reduction and augment in the value of the WS. The value of P_s follows the WS as a result of using the MPPT approach to determine the reference value for this power. This power takes negative values for both controls in the presence of fluctuations, as these fluctuations are less if the designed BC-ALO approach is used compared to the BC approach. Also, it is noted that there is an exceedance of the limit value of P_s , and this exceedance is large in the case of using the BC approach compared to the BC-ALO approach.

The Q_s of the two controllers are represented in Fig. 22. This energy does not change depending on the change in WS, as it takes a fixed value throughout the simulation period. The Q_s take the value 0 VAR as a result of using the MPPT approach, as it is observed that there are fluctuations at the level of this energy for the two controllers. These fluctuations are larger when using the BC approach compared to the BC-ALO approach.

The DC bus voltage for the two techniques is represented in Fig. 23. From this figure, it is noted that the measured value follows the reference well and the value of the DC bus voltage is constant throughout the simulation period and takes the value 1130 V with the presence of fluctuations. Also, the change in DC bus voltage is not affected by the change in WS of the two strategies. DC bus voltage ripples are large when using the

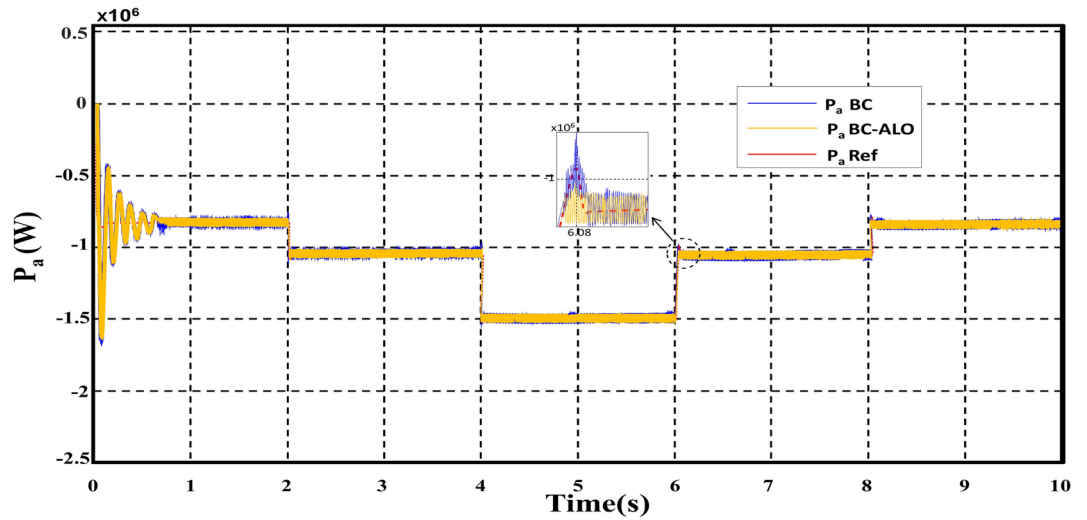


Fig. 21. Active power of a generator in the case of two methods (Third test).

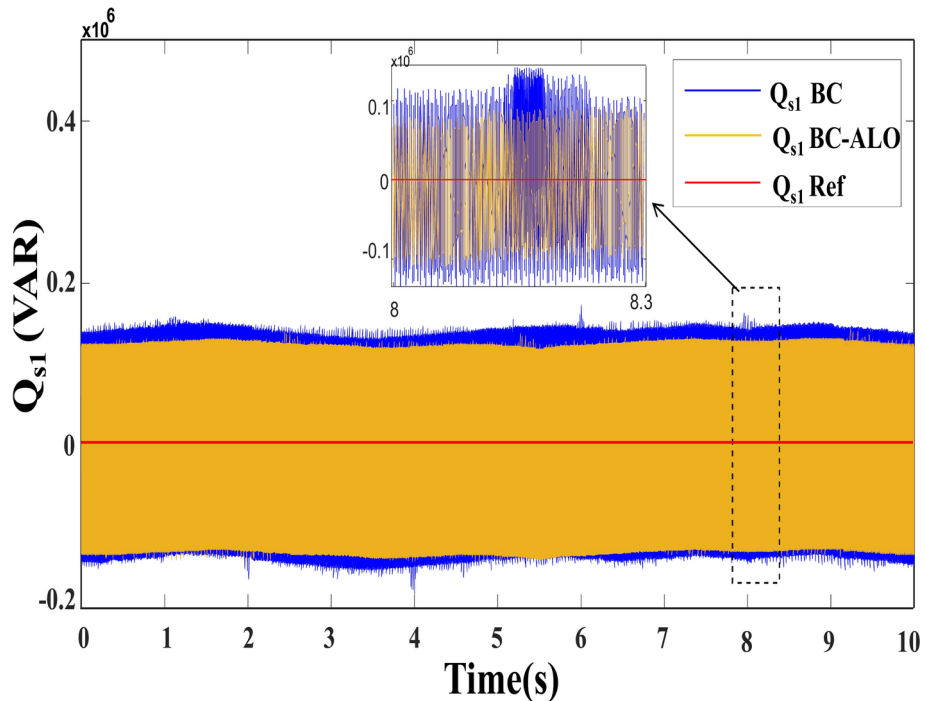


Fig. 22. Active power of the DSIG in the case of two methods (Third test).

BC approach compared to the BC-ALO approach, which is a good thing that shows the extent of the designed strategy’s ability to reduce DC bus voltage ripples.

In Fig. 24, the value of THD and amplitude of FS (50 Hz) current for both techniques is given. Through this form, the value of THD was 1.98% and 3.48% for both the designed BC-ALO strategy and the BC approach, respectively. So, the designed BC-ALO strategy significantly minimized the value of THD compared to the BC approach, which is a positive thing that shows the extent of the ability of the BC-ALO approach to get better the current quality compared to the BC technique. Therefore, the BC-ALO approach reduced the THD by an estimated 43.10% compared to the BC strategy, as this high percentage shows the high efficiency of the BC-ALO approach. Also, it is noted that the amplitude of the FS (50 Hz) for the two controls was equal, which is positive. The value of this amplitude was 1279 A for the two approaches. Therefore, the current quality in this test is high if the BC-ALO approach is used compared to the BC strategy.

The numerical results of this test are represented in Table 6, where it is noted that the BC-ALO approach gave lower values for overshoot, ITAE, and ITSE of P_s compared to the BC technique. Therefore, the BC-

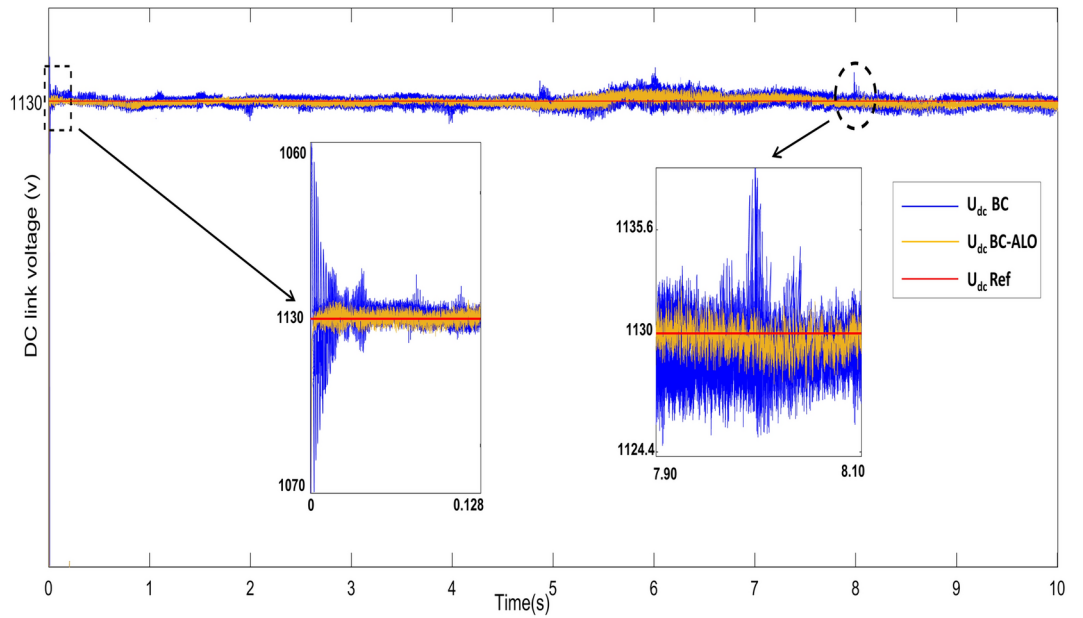


Fig. 23. DC bus voltage of the DSIG (Third test).

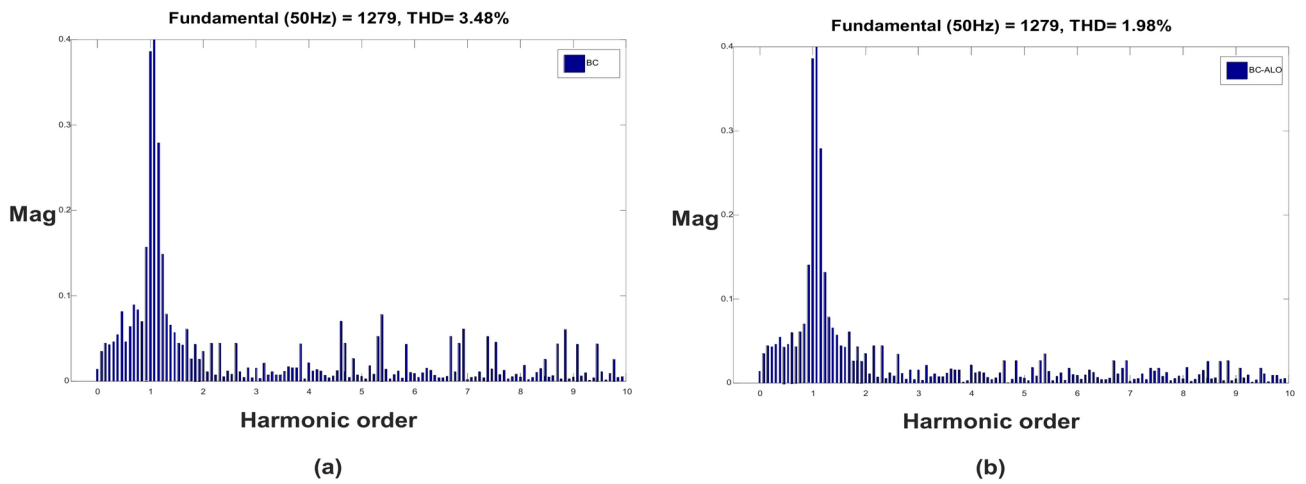


Fig. 24. THD of the current grid (is1g) in the third test: (a) BC and (b) BC-ALO.

Control performances		BC $K_1 = 7.2842e+003$ $K_2 = 7.382e+003$	BC-ALO $K_1 = 5.73261e+003$ $K_2 = 5.1009e+003$	Ratios (%)
$P_s(W)$	ITSE	4.315e+008	2.728e+008	36.77
	ITAE	3.215e+004	1.021e+004	68.24
	Overshoot	2.7313	Negligible	100
	RT (ms)	6.13	3.01	50.89
Q_s	Overshoot	10.3138	Negligible	100
	RT (ms)	128.42	6.18	95.23
V_{dc} ripples		11.1546	3.1348	71.89
THD (%)		3.48	1.98	43.10

Table 6. Performance of both techniques (Third test).

ALO technique reduced the values of overshoot, ITAE, and ITSE by ratios estimated at 100%, 68.24%, and 36.77%, respectively, compared to the BC technique. Also, the BC-ALO technique provided a satisfactory P_s RT compared to the BC technique. The value of this time was 6.13 ms and 3.01 ms for both the BC technique and the BC-ALO technique, respectively. So, the BC-ALO technique reduced the RT of the P_s by an estimated rate of 50.89%, which shows the advantage of the BC-ALO approach in terms of dynamic performance.

The overshoot value for the Q_s was 10.3138 VAR and negligible for both the BC approach and the BC-ALO approach, respectively. Through these values, the BC-ALO approach gave an overshoot value much lower than the BC approach, as the overshoot value was minimized by an estimated ratio of 100%. This high percentage shows the high performance of this designed BC-ALO approach. The RT of the Q_s in the case of using the BC-ALO approach was 6.18 ms, and in the case of the BC approach, its value was estimated at 128.42 ms. So, from these values, it is noted that the BC-ALO approach provided a very small amount of time compared to the BC approach, as this reduction was estimated at a percentage of 95.23%. This ratio shows that the BC-ALO approach has a very fast DR compared to the BC approach. This percentage also shows the efficacy of using the ALO algorithm in improving the features of the studied system.

The BC-ALO approach reduced the V_{dc} ripples compared to the BC approach, as the value of the ripples was 11.1546 V and 3.1348 V for both the BC technique and the BC-ALO approach, respectively. Accordingly, the BC-ALO approach minimized these ripples by an estimated rate of 71.89% compared to the BC approach.

In Table 7, the change in the value of current THD and the value of the amplitude of the FS (50 Hz) between the first and third tests is studied. This table gives the extent to which the value of THD and the amplitude value of the FS (50 Hz) changes with the change in the shape of the WS. From this table, it is noted that the value of both the FS amplitude (50 Hz) and the THD has changed in the third test compared to the first test for the two strategies, where an augment in both values is observed. In the case of the THD value, this augment was estimated at 58.04% and 47.97% for both the BC approach and the BC-ALO approach, respectively. Therefore, the BC-ALO strategy provided a lower rate of increase than the BC approach, which shows that the THD value was more affected when using the BC approach compared to the BC-ALO approach, which enables us to say that the BC-ALO approach is highly efficient in ameliorating the current quality compared to the BC approach. The value of the amplitude of the FS (50 Hz) is significantly affected by the change in the shape of the WS, as this effect appears in the augment in the value of this amplitude in the third test for the two controls. This augment was estimated at 0.31% and 1.01% for both the BC approach and BC-ALO approach, respectively. Accordingly, the BC-ALO approach provided the highest percentage, which indicates the extent of its ability to improve the amplitude value of the FS (50 Hz) compared to the BC approach.

In Table 8, a comparison with other research studies is made in terms of the current THD. This table provides a clear image of the advantage of the BC-ALO approach over other techniques, which is a positive finding that indicates its distinguished performance in terms of enhancing the current quality. Notably, the results in this table suggest that the BC-ALO approach can be used in the future in the area of control.

Conclusions

In this work, a suitable and effective solution is proposed to improve the power quality and robustness of the control system based on the use of DFIG. The proposed solution depends on improving the performance and effectiveness of the backstepping control strategy using the ALO algorithm. The proposed solution is characterized by high performance, ease of application, and great robustness. In addition to using improved backstepping control, the PWM strategy was used to control the operation of the system's inverters. The parameters of the proposed approach were calculated using the ALO algorithm. The proposed approach was compared with the traditional strategy in terms of power quality, THD value of current, overshoot, steady-state error, and response time. Also, the proposed approach was compared with related works in terms of the THD of current value. In this work, MATLAB was relied upon to implement the proposed approach, where two different forms of wind speed were used to prove the effectiveness and strength of this proposed approach. The results show that the proposed technique provides graphical and numerical results compared to the conventional technique, as it provided good numerical results in terms of the values of ITSE, ITAE, response time, overshoot, and DC link voltage ripples. Results in all tests show that the proposed technique minimized the THD value by percentages estimated at 43.10%, 57.25%, and 29.45% compared to the conventional technique. Additionally, the DC link voltage ripples were reduced compared to the conventional technique by 71.89%, 71.38%, and 63.31% in all

		Techniques	
		BC	BC-ALO
THD of the current (A)	First test	1.46	1.03
	Third test	3.48	1.98
	Third test-First test	2.02	0.95
	Ratios	58.04%	47.97%
Amplitude of the FS of the current (A)	First test	1283	1292
	Third test	1279	1279
	Third test-First test	4	13
	Ratios	0.31%	1.01%

Table 7. Changes in the THD and amplitude of the FS (50 Hz) during the first and third tests.

References		THD (%)
23	SMC	85.26
	STCSMC	62.38
18		3.3
26		1.62
30		3.56
31	SMC	85.26
	Second-order SMC	70.59
	TOSMC	58.18
32	Test 1	1.39
	Test 2	1.46
71		5.8
BC-ALO	Test 1	1.12
	Test 2	1.03
	Test 3	1.98

Table 8. Comparison of the designed control and other controls in terms of the current THD.

tests. Compared to the conventional strategy, the proposed approach reduced the response time to active power compared to the conventional technique by approximately 50.89%, 53.44%, and 0.60% in all tests. Also, the response time for reactive power was reduced by 95.23%, 97.78%, and 97.65% in all tests performed. These results prove that the proposed technique significantly increases the strength and robustness of the DFIG-based wind turbine system compared to using the conventional technique.

In this work, simulation was relied upon only to highlight the performance and effectiveness of the proposed approach due to the lack of necessary equipment. This challenge will be addressed in other works in the future. In addition, the lack of relevant work related to the DFIG-type generator is considered one of the most prominent challenges that this work faced in comparing the results. Also, this system relied only on power generation while increasing the power quality. The energy storage system was not addressed, which creates the problem or challenge of energy surplus in this work. Therefore, in future work, this work will be attempted experimentally using real tools and a storage system. Also, another control proposal is characterized by high performance and great durability, with a focus on simplicity and ease of implementation to control powers.

Data availability

Data available on request from the authors. The datasets used and/or analysed during the current study available from the corresponding author on reasonable request. In the event of communication, the third author (Habib Benbouhenni, E-mail: habib.benbouhenni@enp-oran.dz) will respond to any inquiry or request.

Received: 3 January 2025; Accepted: 7 April 2025

Published online: 18 April 2025

References

- Abdelfattah, D., Mohamed, B., Zineb, M., Mhamed, E. & Mohammed, B. Wind energy conversion technologies and control strategies: A review. *Int. J. Renew. Energy Res.* **14**(1), 140–154. <https://doi.org/10.20508/ijrer.v14i1.14296.g8869> (2024).
- Reza, G., Ali, M. & Alireza Davari, S. A new control algorithm method based on DPC to improve power quality of DFIG in unbalance grid voltage conditions. *Int. J. Renew. Energy Res.* **8**(4), 2228–2238. <https://doi.org/10.20508/ijrer.v8i4.8583.g7527> (2018).
- Ngoc, A. V. & Ngoc, S. P. An analytical methodology for aerodynamic analysis of vertical axis wind turbine. *Int. J. Renew. Energy Res.* **10**(3), 1145–1153. <https://doi.org/10.20508/ijrer.v10i3.11001.g7988> (2020).
- Abdelhakim, B., Ilhami, C., Korhan, K. & Ramazan, B. Modeling of a permanent magnet synchronous generator in a power wind generation system with an electrochemical energy storage. *Int. J. Smart Grid* **2**(4), 197–202 (2018).
- Yu, L., Zhang, Z., Chen, Z. & Yan, Y. Analysis and verification of the doubly salient brushless DC generator for automobile auxiliary power unit application. *IEEE Trans. Ind. Electron.* **61**(12), 6655–6663. <https://doi.org/10.1109/TIE.2014.2320224> (2014).
- Faisal, R. B., Subrata, K. S. & Sajal, K. D. Transient stabilization improvement of induction generator based power system using robust integral linear quadratic gaussian approach. *Int. J. Smart Grid* **3**(2), 73–83. <https://doi.org/10.20508/ijsmartgrid.v3i2.60.g48> (2019).
- Teymoori, V., Kamper, M., Wang, R.-J. & Kennel, R. Sensorless control of dual three-phase permanent magnet synchronous machines—A review. *Energies* **16**, 1326. <https://doi.org/10.3390/en16031326> (2023).
- Lounnas, F., Haddad, S. & Fekik, A. Twin stator induction generator power control with PI regulators for wind energy conversion system. In *Power Electronics Converters and their Control for Renewable Energy Applications* 115–144. <https://doi.org/10.1016/B978-0-323-91941-8.00006-8> (Academic Press, 2020).
- Jose Antonio, B.-R., Juan Ignacio, T. & Luis, M.-S. Variable-speed wind energy conversion system based on a dual stator-winding induction generator. *IET Renew. Power Gener.* **11**(1), 73–80. <https://doi.org/10.1049/iet-rpg.2016.0186> (2017).
- Singh, G. K., Senthil Kumar, A. & Saini, R. P. A self-excited six-phase induction generator for stand-alone renewable energy generation: experimental analysis. *Eur. Trans. Electric Power* **20**(7), 884–900. <https://doi.org/10.1002/etep.372> (2010).
- Bentley, R. E. *Handbook of Temperature Measurement Vol. 3: The Theory and Practice of Thermoelectric Thermometry* (Springer, 1998).
- Mohd, F. K. & Mohd, R. K. Generalized model for investigating the attributes of a six-phase self-excited induction generator over a three-phase variant. *Int. Trans. Electric Energy Syst.* **28**(10), e2600. <https://doi.org/10.1002/etep.2600> (2018).

13. Changguo, Z., Ming, C. & Yu, Z. Design and analysis of dual-stator brushless doubly-fed generator for wind turbine. *IEEE Trans. Electr. Electron. Eng.* **17**(2), 276–286. <https://doi.org/10.1002/tee.23503> (2022).
14. Samuli, K., Jussi, K., Pasi, P., Pertti, S. & Olli, P. Determination of the inductance parameters for the decoupled d–q model of double-star permanent-magnet synchronous machines. *IET Electr. Power Appl.* **8**(2), 39–49. <https://doi.org/10.1049/iet-epa.2013.0195> (2014).
15. Iffouz, K. et al. A new post-fault reconfiguration strategy under open-phase operation conditions of asymmetrical double-star induction machines. *Energies* **16**, 5740. <https://doi.org/10.3390/en16155740> (2023).
16. Benbouya, B. et al. Sliding mode control of an electric vehicle driven by a new powertrain technology based on a dual-star induction machine. *World Electr. Veh. J.* **15**, 155. <https://doi.org/10.3390/wevj15040155> (2024).
17. Iqbal, A. & Singh, G. K. PSO based controlled six-phase grid connected induction generator for wind energy generation. *CES Trans. Electric. Mach. Syst.* **5**(1), 41–49. <https://doi.org/10.30941/CESTEMS.2021.00006> (2021).
18. Benakcha, M., Benalia, L., Ameer, F. & Tourqui, D. E. Control of dual stator induction generator integrated in wind energy conversion system. *J. Energy Syst.* **1**(1), 21–31. <https://doi.org/10.30521/jes.351269> (2017).
19. Chinmaya, K. A. & Girish, K. S. Performance evaluation of multiphase induction generator in stand-alone and grid-connected wind energy conversion system. *IET Renew. Power Gener.* **12**(7), 823–831. <https://doi.org/10.1049/iet-rpg.2017.0791> (2018).
20. Shantanu, C., Arghya, M. & Abhijit, D. Air-gap flux-oriented vector control of dual stator induction generator used in wind energy conversion system with novel 13-zone time optimized space vector-based hybrid bus clamping PWM. *Int. Trans. Electric. Energy Syst.* **31**(12), e13217. <https://doi.org/10.1002/2050-7038.13217> (2021).
21. Chekkal, S., Lahaçani, N. A., Aouzellag, D. & Ghedamsi, K. Fuzzy logic control strategy of wind generator based on the dual-stator induction generator. *Int. J. Electr. Power Energy Syst.* **59**, 166–175. <https://doi.org/10.1016/j.ijepes.2014.02.005> (2014).
22. Shantanu, C. & Saibal, C. Stator flux-oriented vector control of dual stator induction generator with time optimized 11-zone hybrid PWM for grid connected wind energy generation system. *IET Electr. Power Appl.* **13**(11), 1835–1848. <https://doi.org/10.1049/iet-e-pa.2018.5311> (2019).
23. Guettab, A., Boudjema, Z., Bounadja, E. & Taleb, R. Improved control scheme of a dual star induction generator integrated in a wind turbine system in normal and open-phase fault mode. *Energy Rep.* **8**, 6866–6875. <https://doi.org/10.1016/j.egy.2022.05.048> (2022).
24. Moati, Y., Katia, K. & Mokhtari, K. Improvement of DTC of wind energy conversion system based on DSIG using matrix converter. In *2019 1st International Conference on Sustainable Renewable Energy Systems and Applications (ICSRESA), Tebessa, Algeria, 2019* 1–6. <https://doi.org/10.1109/ICSRESA49121.2019.9182509> (2019).
25. Wang, X. & Wu, X. Research on dual-stator winding multi-phase generator with rectifier load. *Sci. China Ser. E Technol. Sci.* **51**, 683–692. <https://doi.org/10.1007/s11431-008-0052-6> (2008).
26. Mesai-ahmed, H., Bentaallah, A., Cardoso, A. J. M., Djeriri, Y. & Jlassi, I. Robust neural control of the dual star induction generator used in a grid-connected wind energy conversion system. *Math. Model. Eng. Probl.* **8**(3), 323–332. <https://doi.org/10.18280/mmp.080301> (2021).
27. Fatma, L., Salah, H. & Arezki, F. Chapter 6—Twin stator induction generator power control with PI regulators for wind energy conversion system. In *Power Electronics Converters and their Control for Renewable Energy Applications* 115–144. <https://doi.org/10.1016/B978-0-323-91941-8.00006-8> (2023).
28. Hamitouche, K., Chekkal, S., Amimeur, H. & Aouzellag, D. A new control strategy of dual stator induction generator with power regulation. *J. Eur. Syst. Autom.* **53**(4), 469–478. <https://doi.org/10.18280/jesa.530404> (2020).
29. Kamal, N., Khoudir, M., Mohamed, B. & Bekheira, T. DC bus voltage control of a power generation system based on a dual star induction generator. *Int. Rev. Electric. Eng.* **11**(6), 69. <https://doi.org/10.15866/iree.v11i6.9769> (2016).
30. Meryem, B. Backstepping control of dual stator induction generator used in wind energy conversion system. *Int. J. Renew. Energy Res.* **8**(1), 1 (2018).
31. Guettab, A., Bounadja, E., Boudjema, Z. & Taleb, R. Third-order super-twisting control of a double stator asynchronous generator integrated in a wind turbine system under single-phase open fault. *Int. J. Circuit Theory Appl.* **51**(4), 1858–1878. <https://doi.org/10.1002/cta.3511> (2023).
32. Abdessmad, M., Elkheir, M., Habib, B., Naamane, D. & Ilhami, C. Robust control technique for wind turbine system with interval type-2 fuzzy strategy on a dual star induction generator. *Energy Rep.* **11**, 2715–2736. <https://doi.org/10.1016/j.egy.2024.01.060> (2024).
33. Shantanu, C. & Saibal, C. A novel speed sensor-less vector control of dual stator induction machine with space vector based advanced 9-zone hybrid PWM for grid connected wind energy generation system. *Electr. Power Syst. Res.* **163**, 174–195. <https://doi.org/10.1016/j.epsr.2018.02.021> (2018).
34. Alanis, A. Y., Sanchez, E. N. & Loukianov, A. G. Real-time discrete backstepping neural control for induction motors. *IEEE Trans. Control Syst. Technol.* **19**(2), 359–366. <https://doi.org/10.1109/TCST.2010.2041780> (2011).
35. Makhad, M., Zazi, M., Loulijat, A. & Simon, A. O. Robust Integral backstepping control for optimal power extraction of a PMSG-based variable speed wind turbines. In *2020 1st International Conference on Innovative Research in Applied Science, Engineering and Technology (IRASET), Meknes, Morocco* 1–6. <https://doi.org/10.1109/IRASET48871.2020.9092053> (2020).
36. Xiong, P. & Sun, D. Backstepping-based DPC strategy of a wind turbine-driven DFIG under normal and harmonic grid voltage. *IEEE Trans. Power Electron.* **31**(6), 4216–4225. <https://doi.org/10.1109/TPEL.2015.2477442> (2016).
37. Zellouma, D., Habib, B. & Bekakra, Y. Backstepping control based on a third-order sliding mode controller to regulate the torque and flux of asynchronous motor drive. *Period. Polytech. Electr. Eng. Comput. Sci.* **67**(1), 10–20. <https://doi.org/10.3311/PPee.20333> (2023).
38. Bossoufi, B. et al. Rooted tree optimization for the backstepping power control of a doubly fed induction generator wind turbine: dSPACE implementation. *IEEE Access.* **9**, 26512–26522. <https://doi.org/10.1109/ACCESS.2021.3057123> (2021).
39. Habib, B., Gasmii, H. & Colak, I. Backstepping control for multi-rotor wind power systems. *Majlesi J. Energy Manag.* **11**(4), 8–15 (2022).
40. Debdouche, N., Zarour, L., Benbouhenni, H., Mehazzem, F. & Deffaf, B. Robust integral backstepping control microgrid connected photovoltaic system with battery energy storage through multi-functional voltage source inverter using direct power control SVM strategies. *Energy Rep.* **10**, 565–580. <https://doi.org/10.1016/j.egy.2023.07.012> (2023).
41. Adil, Y., Habib, B., Ilhami, C. & Nicu, B. Application of backstepping control with nonsingular terminal sliding mode surface technique to improve the robustness of stator power control of asynchronous generator-based multi-rotor wind turbine system. In *Electric Power Components and Systems* 1–19. <https://doi.org/10.1080/15325008.2024.2304688> (2024).
42. Abdelkader, A. et al. Robust Lyapunov-based power controllers with integral action for a wind farm. In *Electric Power Components and Systems* 1–36. <https://doi.org/10.1080/15325008.2024.2311880> (2024).
43. Dalal, Z., Youcef, B. & Habib, B. Robust synergetic-sliding mode-based-backstepping control of induction motor with MRAS technique. *Energy Rep.* **10**, 3665–3680. <https://doi.org/10.1016/j.egy.2023.10.035> (2023).
44. Benbouhenni, H. Application of DPC and DPC-GA to the dual-rotor wind turbine system with DFIG. *Int. J. Robot. Autom.* **10**(3), 224–234. <https://doi.org/10.11591/ijra.v10i3.pp224-234> (2021).
45. Gasmii, H., Sofiane, M., Benbouhenni, H. & Bizon, N. Optimal operation of doubly-fed induction generator used in a grid-connected wind power system. *Iran. J. Electric. Electron. Eng.* **19**(2), 2431–2431. <https://doi.org/10.22068/IJEEE.19.2.2431> (2023).
46. Wu, L., Zhao, D., Zhao, X. & Qin, Y. Nonlinear adaptive back-stepping optimization control of the hydraulic active suspension actuator. *Processes* **11**, 2020. <https://doi.org/10.3390/pr11072020> (2023).

47. Laihong, Z., Juqian, Z., Jingxin, D. & Bangchun, W. A fuzzy adaptive backstepping control based on mass observer for trajectory tracking of a quadrotor UAV. *Int. J. Adapt. Control Signal Process.* **32**(12), 1675–1693. <https://doi.org/10.1002/acs.2937> (2018).
48. Chih-Hong, L. & Kuo-Tsai, C. Switched reluctance motor circuit drive system using adaptive nonlinear backstepping control with mended recurrent Romanovski polynomials neural network and mended particle swarm optimization. *Int. J. Numer. Model. Electron. Netw. Devices Fields* **32**(5), e2629. <https://doi.org/10.1002/jnm.2629> (2019).
49. Qi, T., Dezhi, X., Weilin, Y., Jianlin, L. & Peng, S. Neural network-based integral sliding mode backstepping control for virtual synchronous generators. *Energy Rep.* **7**, 1–9. <https://doi.org/10.1016/j.egy.2020.11.032> (2021).
50. Assia, H. et al. Wind turbine active fault tolerant control based on backstepping active disturbance rejection control and a neuro fuzzy detector. *Energies* **16**, 5455. <https://doi.org/10.3390/en16145455> (2023).
51. Lin, F.-J., Huang, M.-S., Chien, Y.-C. & Chen, S.-G. Intelligent backstepping control of permanent magnet-assisted synchronous reluctance motor position servo drive with recurrent wavelet fuzzy neural network. *Energies* **16**, 5389. <https://doi.org/10.3390/en16145389> (2023).
52. Yuehui, J., Hailiang, Z. & Qun, Z. Adaptive neural network command filtered backstepping control of pure-feedback systems in presence of full state constraints. *Int. J. Adapt. Control Signal Process.* **33**(5), 829–842. <https://doi.org/10.1002/acs.2989> (2019).
53. Yongchao, W., Lijia, C., Shengxiu, Z., Xiaoxiang, H. & Feixiong, Y. Command filtered adaptive fuzzy backstepping control method of uncertain non-linear systems. *IET Control Theory Appl.* **10**(10), 1134–1141. <https://doi.org/10.1049/iet-cta.2015.0946> (2016).
54. Es-saadi, T., Sofiane, M., Salah Eddine, R., Hamza, G. & Walid, K. Optimal third-order sliding mode controller for dual star induction motor based on grey wolf optimization algorithm. *Heliyon*. **10**(12), e32669. <https://doi.org/10.1016/j.heliyon.2024.e32669> (2024).
55. Alouane, A. & Khedher, A. SVPWM Algorithm for a Delta Inverters-Fed Double-Star Induction Machine. *7th IEEE International Power Electronics Congress. Technical Proceedings. CIEP 2000 (Cat. No. 00TH8529)* 42–47. <https://doi.org/10.1109/SSD49366.2020.9364154> (IEEE, 2000).
56. Chakib, M., Tamou, N. & Ahmed, E. Contribution of variable speed wind turbine generator based on DFIG using ADRC and RST controllers to frequency regulation. *Int. J. Renew. Energy Res.* **11**(1), 320–331. <https://doi.org/10.20508/ijrer.v11i1.11762.g8136> (2021).
57. Farida, M., Sebti, B. & Ilhami, C. DPC-SVM of DFIG using fuzzy second order sliding mode approach. *Int. J. Smart Grid* **5**(4), 174–182. <https://doi.org/10.20508/ijsmartgrid.v5i4.219.g178> (2021).
58. Rayane, L. & Lekhchine, S. Fuzzy logic controller-based power control of DFIG based on wind energy systems. *Int. J. Smart Grid* **8**(1), 74–80. <https://doi.org/10.20508/ijsmartgrid.v8i1.334.g346> (2024).
59. Harish, V. S. K. V. & Sant, A. V. Grid integration of wind energy conversion systems. In *Alternative Energy Resources: The Way to a Sustainable Modern Society* 45–66. https://doi.org/10.1007/978-2020_610 (2021).
60. Sumanth, Y., Lakshminarasimman, L. & Sambasiva Rao, G. Optimal design of FoPID controller for DFIG based wind energy conversion system using Grey-Wolf optimization algorithm. *Int. J. Renew. Energy Res.* **12**(4), 2111–2120. <https://doi.org/10.20508/ijrer.v12i4.13446.g8594> (2022).
61. Moez, A., Sahbi, A., Habib, B. Z. & Mohamed, C. A novel fuzzy control strategy for maximum power point tracking of wind energy conversion system. *Int. J. Smart Grid* **3**(3), 120–127. <https://doi.org/10.20508/ijsmartgrid.v3i3.63.g58> (2019).
62. Rami Reddy, C., Naresh, K., Umapathi Reddy, P. & Sujatha, P. Control of DFIG based wind turbine with hybrid controllers. *Int. J. Renew. Energy Res.* **10**(3), 1488–1500. <https://doi.org/10.20508/ijrer.v10i3.11010.g8028> (2020).
63. Mohammed, F., Ahmed, E., Mohamed, N. & Tamou, N. Control and optimization of a wind energy conversion system based on doubly-fed induction generator using nonlinear control strategies. *Int. J. Renew. Energy Res.* **9**(1), 44–45. <https://doi.org/10.20508/ijrer.v9i1.8812.g7619> (2019).
64. Wahabi, A., Elmoudden, A. & Senhaji Rhazi, K. Use of a doubly-fed induction generator for the conversion of wind energy. In *International Conference on Digital Technologies and Applications* 1245–1253. https://doi.org/10.1007/978-3-030-73882-2_114 (Springer, 2021).
65. Bossoufi, B. et al. Observer Backstepping control of DFIG-generators for wind turbines variable-speed: FPGA-based implementation. *Renew. Energy* **81**, 903–917. <https://doi.org/10.1016/j.renene.2015.04.013> (2015).
66. Benakcha, M., Benakcha, A. & Ammar, A. Backstepping Sliding mode control of DFIG driven by variable speed wind turbine. In *2022 19th International Multi-Conference on Systems, Signals & Devices (SSD), Sétif, Algeria, 2022* 296–302. <https://doi.org/10.1109/SSD54932.2022.9955775> (2022).
67. Abualigah, L. et al. Ant lion optimizer: A comprehensive survey of its variants and applications. *Arch. Comput. Methods Eng.* **28**, 1397–1416. <https://doi.org/10.1007/s11831-020-09420-6> (2021).
68. Bouyahia, O., Betin, F. & Yazidi, A. Optimal sliding mode control of a symmetrical six-phase induction generator for wind turbines. *IEEE Trans. Ind. Appl.* **85**(6), 7308–7317. <https://doi.org/10.1109/TIA.2022.3195971> (2022).
69. Guo, M. W. et al. Improved ant lion optimizer based on spiral complex path searching patterns. *IEEE Access.* **8**, 22094–22126 (2020).
70. Hamza, G., Habib, B., Sofiane, M. & Ilhami, C. A new scheme of the fractional-order super twisting algorithm for asynchronous generator-based wind turbine. *Energy Rep.* **9**, 6311–6327. <https://doi.org/10.1016/j.egy.20> (2023).
71. Khan, M. F. & Khan, M. R. Generalized model for investigating the attributes of a six-phase self-excited induction generator over a three-phase variant. *Int. Trans. Electric. Energy Syst.* **28**(10), e2600. <https://doi.org/10.1002/etep.2600> (2018).

Author contributions

Conceptualization: Abdessmad Milles, Elkheir Merabet, Habib Benbouhenni, Ilhami Colak; methodology: Abdessmad Milles, Elkheir Merabet, Habib Benbouhenni, Mohammed-Salah Aggoune and Ghoulemallah Boukhalfa; software: Abdessmad Milles, Habib Benbouhenni, Ilhami Colak, Nouredine Bensedira, Naamane Debouche; validation: Abdessmad Milles, Habib Benbouhenni, Nouredine Bensedira, Naamane Debouche formal analysis: Abdessmad Milles, Habib Benbouhenni, Ilhami Colak, Nouredine Bensedira, Naamane Debouche, Mohammed-Salah Aggoune and Ghoulemallah Boukhalfa; investigation: Abdessmad Milles, Habib Benbouhenni, Naamane Debouche, Mohammed-Salah Aggoune and Ghoulemallah Boukhalfa; resources: Abdessmad Milles, Habib Benbouhenni, Ilhami Colak, Nouredine Bensedira, Mohammed-Salah Aggoune and Ghoulemallah Boukhalfa; data curation: Abdessmad Milles, Habib Benbouhenni, Ilhami Colak, Nouredine Bensedira, Naamane Debouche; writing—original draft preparation: Abdessmad Milles, Habib Benbouhenni, Ilhami Colak; writing—review and editing: Elkheir Merabet, Habib Benbouhenni, Ilhami Colak, Nouredine Bensedira, Mohammed-Salah Aggoune and Ghoulemallah Boukhalfa; visualization: Elkheir Merabet, Habib Benbouhenni, Ilhami Colak, Nouredine Bensedira, Naamane Debouche, Mohammed-Salah Aggoune and Ghoulemallah Boukhalfa; supervision: Abdessmad Milles, Elkheir Merabet, Habib Benbouhenni, Ilhami Colak, Nouredine Bensedira, Naamane Debouche, Mohammed-Salah Aggoune and Ghoulemallah Boukhalfa; project administration: Abdessmad Milles, Elkheir Merabet, Habib Benbouhenni, Ilhami Colak; funding acquisition: Habib Benbouhenni, Ilhami Colak All authors have read and agreed to the published version of the

manuscript.

Competing interests

The authors declare no competing interests.

Additional information

Correspondence and requests for materials should be addressed to H.B.

Reprints and permissions information is available at www.nature.com/reprints.

Publisher's note Springer Nature remains neutral with regard to jurisdictional claims in published maps and institutional affiliations.

Open Access This article is licensed under a Creative Commons Attribution-NonCommercial-NoDerivatives 4.0 International License, which permits any non-commercial use, sharing, distribution and reproduction in any medium or format, as long as you give appropriate credit to the original author(s) and the source, provide a link to the Creative Commons licence, and indicate if you modified the licensed material. You do not have permission under this licence to share adapted material derived from this article or parts of it. The images or other third party material in this article are included in the article's Creative Commons licence, unless indicated otherwise in a credit line to the material. If material is not included in the article's Creative Commons licence and your intended use is not permitted by statutory regulation or exceeds the permitted use, you will need to obtain permission directly from the copyright holder. To view a copy of this licence, visit <http://creativecommons.org/licenses/by-nc-nd/4.0/>.

© The Author(s) 2025